

Monitoring the Formation and Reactivity of Organometallic Alkane and Fluoroalkane Complexes with Silanes and Xe Using Time-resolved XAFS

Stuart A. Bartlett^{1,2,3}, Nicholas A. Besley,⁴ Andrew J. Dent,⁵ Sofia Diaz-Moreno,⁵ John Evans,^{1,5,6} Michelle L. Hamilton^{1,4}, Magnus W. D. Hanson-Heine,⁴ Raphael Horvath,⁴ Valentina Manici,^{1,4} Xue-Zhong Sun,⁴ Michael Towrie,^{1,7} Lingjun Wu,⁴ Xiaoyi Zhang⁸ and Michael W. George,^{1,4,9}

¹DySS, Research Complex at Harwell, Rutherford Appleton Laboratory, Didcot, OX11 0FA, UK

²School of Chemistry, The University of Sydney, Eastern Ave, Sydney NSW 2006, Australia

³Department of Chemistry, University of Bath, Claverton Down, Bath, BA2 7AY, United Kingdom

⁴School of Chemistry, University of Nottingham, University Park NG7 2RD, United Kingdom

⁵Diamond Light Source, Rutherford Appleton Laboratory, Didcot, OX11 0DE, United Kingdom

⁶Chemistry, University of Southampton, Southampton, SO17 1BJ, UK.

⁷Central Laser Facility, Research Complex at Harwell, Rutherford Appleton Laboratory, Chilton, Oxfordshire OX11 0QX, United Kingdom

⁸X-ray Science Division, Argonne National Laboratory, Argonne, USA

⁹Department of Chemical and Environmental Engineering, University of Nottingham Ningbo China, 199 Taikang East Road, Ningbo 315100, China

Abstract: Complexes with weakly coordinating ligands are often formed in chemical reactions and can play key roles in determining the reactivity, particularly in catalytic reactions. Using time-resolved XAFS in combination with time-resolved IR (TRIR) spectroscopy and tungsten hexacarbonyl, $W(CO)_6$, we are able to structurally characterise the formation of an organometallic alkane complex, determine the W-C distances and monitor the reactivity with silane to form an organometallic silane complex. Experiments in perfluorosolvents doped with xenon afford initially the corresponding solvated complex which is sufficiently reactive in the presence of Xe that we can then observe the coordination of Xe to the metal centre, providing a unique insight into the metal-xenon bonding. These results offer a step toward elucidating the structure, bonding and chemical reactivity of transient species by X-ray absorption spectroscopy, which has sensitivity to small structural changes. The XAFS results indicate that the bond lengths of metal-alkane (W-H-C) bond in $W(CO)_5(\text{heptane})$ as $3.07 (\pm 0.06) \text{ \AA}$ which is longer than the calculated W-C (2.86 \AA) for binding of the primary C-H but shorter than the calculated W-C (3.12 \AA) for the secondary C-H. A statistical average of the calculated W-C alkane bond length is 3.02 \AA and comparison of this value indicates that experiment the value derived from the XAFS measurements is averaged over coordination of all C-H bonds consistent with alkane chain walking. Photolysis of $W(CO)_6$ in the presence of $HSiBu_3$ allows the the conversion of $W(CO)_5(\text{heptane})$ to $W(CO)_5(HSiBu_3)$ with an estimated W-Si distance of $3.20 (\pm 0.03) \text{ \AA}$. Time-resolved TRIR and XAFS experiments following photolysis of $W(CO)_6$ in perfluoromethylcyclohexane (PFMCH) allows the characterisation of $W(CO)_5(\text{PFMCH})$ with a W-F distance of $2.65 (\pm 0.06) \text{ \AA}$ and doping PFMCH with Xe allows the characterisation of $W(CO)_5Xe$ with a W-Xe bond length of $3.10 (\pm 0.02) \text{ \AA}$.

Introduction

It is now more than 40 years since the first reported evidence for the interaction of $M(\text{CO})_5$ ($M = \text{Cr}, \text{Mo}$ and W) with noble gases and CH_4 in matrices at cryogenic temperatures.¹ These pioneering low temperature spectroscopic experiments provided the first strong circumstantial evidence through infrared and UV/visible spectroscopy for the existence of organometallic alkane complexes, which are now widely known as σ -complexes, and also in the coordination of noble gases which are some of the most weakly coordinating ligands. These σ -complexes continue to challenge the nature of metal ligand bonding. σ -complexes can be formed between transition metals and ligands such as dihydrogen, borane, silane and germane forming an important class of compounds both for their chemical bonding and as intermediates in catalytic processes.² Elucidating the structure, bonding and reactivity of these compounds is a prerequisite for full understanding of such processes. Although organometallic alkane complexes are less extensively characterised than other σ -complexes, they have been shown to be reaction intermediates in many fundamental transformations associated with transition metal centres. These include oxidative addition/reductive elimination, protonation, σ -complex assisted metathesis (σ -CAM), hydrogenation/dehydrogenation and substitution reactions.³ Many σ -complexes such as metal-dihydrogen, metal-borane, and metal-silane have been studied extensively by a whole range of spectroscopic and diffraction methods as well as by extensive theoretical studies. However, obtaining structural information about organometallic alkane complexes is experimentally much more difficult, and mostly rely on solution spectroscopic and kinetic information has been derived from room temperature time-resolved UV/vis and IR spectroscopy,⁴ and mass spectrometry.⁵ Low-temperature solution NMR spectroscopic studies have provided information on only a few alkane complexes⁶ and currently only on a single example of a xenon complex.⁷ In the solid state there has been evidence from X-ray crystallography⁸ and powder neutron diffraction studies at 4–8K⁹ for alkane binding in a few selected examples. The breakthrough in characterising a well-defined σ -alkane complex came from the use of solid/gas single-crystal to single-crystal transformations to allow the X-ray crystallographic characterisation of $[\text{Rh}(\text{R}_2\text{PCH}_2\text{CH}_2\text{PR}_2)(\eta^2:\eta^2\text{-NBA})][\text{BArF}_4]$ (NBA = norbornane; $\text{R} = \text{iBu}$, or Cy ; $\text{ArF} = 3,5\text{-(CF}_3)_2\text{C}_6\text{H}_3$), by addition of H_2 to the diene precursor $[\text{Rh}(\text{R}_2\text{PCH}_2\text{CH}_2\text{PR}_2)(\eta^2:\eta^2\text{-NBD})][\text{BArF}_4]$ (NBD = norbornadiene).¹⁰ Although organometallic xenon complexes have not been extensively studied, a stable metal-xenon complex has been reported following reduction of AuF_3 by elemental xenon in HF/SbF_5 solution, resulting in the formation of $[\text{AuXe}_4^{2+}][\text{Sb}_2\text{F}_{11}]^{2-}$ which was characterised by X-ray crystallography.¹¹ In solution the application of NMR for structural characterisation is limited in time-resolved measurements as the transient species have to be long-lived for

these measurements. In this paper, we use time-resolved X-ray absorption fine structure (XAFS) spectroscopy to examine the formation and reactivity of organometallic alkane and noble gas complexes and monitor the reactivity of metal alkane with silanes to form complexes since these have been extensively studied by other methods and they they are key to many catalytic transformations.¹²

Time-resolved X-ray absorption fine structure (XAFS) spectroscopy has a long history for studying structure-reactivity studies in chemistry and recently there has been increased interest in the application of this technique to unstable complexes.¹³ The XAFS spectra can provide a detailed electronic and structural picture through XANES (X-ray absorption near edge structure) and EXAFS (extended X-ray absorption fine structure) with added time resolution, limited by the X-ray photon bunch length and count-rate together with the detection method. Today, measurements can be made on the femtosecond timescale. Because of this, many of the time-resolved XAFS studies have focussed on elucidating the structure and reactivity of excited states in transition metal systems partly because these challenging measurements are helped by high quantum yield processes in these experiments. The analysis of difference EXAFS data has been attempted less frequently as the modulations are significantly weaker than the signal collected in the XANES region. An early example of structural elucidation via transient EXAFS data involved the photochemically induced spin-crossover complex of $[\text{Fe}(\text{II})(\text{bpy})_3]^{2+}$ (bpy = bipyridyl). Analysis of these data provided highly accurate information about bond distance changes at 50 picoseconds.¹⁴ The structural analysis employed a method to calculate a series of EXAFS spectra with stepwise increasing distances between the Fe central atom and the bpy ligands. This methodology also provided reasonable values for the chemical energy shift in the absorption edge between both states. In the case of $[\text{Fe}(\text{bpy})_3]^{2+}$, only one Fe-ligand distance is changing. This same approach has also been used to determine more than one type of bond structure change, achieved in the EXAFS analysis of the triplet excited state of $[\text{Pt}_2(\text{P}_2\text{O}_5\text{H}_2)_4]^{4-}$ in solution at 150 nanoseconds¹⁵ having previously been studied on the microsecond timescale in one of the earliest pump-probe XAFS studies.¹⁶ Recently, the displacement of Zn in the regular lattice of ZnO after photoexcitation was also observed through O-Zn bond distance changes after 80 picoseconds.¹⁷ Other notable studies have been described¹⁸ including the experimental fitting of changing Ce-O bonding with and without an electric field and monitoring the strain of a FeCo film under magnetorestriction. A theoretical analysis on a reaction system was also conducted detailing the potential analysis of the oxidation of ruthenium nanoparticles upon exposure to O_2 or H_2 .

Here we use a data analysis method using the EXAFS data analysis software package Artemis (IFEFFIT),¹⁹ and combined with time resolved IR data and DFT calculations, we report the use of time-resolved XAFS to reveal evidence for the organometallic tungsten-xenon interaction in $\text{W}(\text{CO})_5\text{Xe}$, and also

bond distances in $W(CO)_5(HSiBu_3)$ and $W(CO)_5(\text{alkane})$ photoproducts from $W(CO)_6$ starting material, complexes that otherwise could not be structurally resolved.

Experimental

Materials and methods

All solvents were purchased from Aldrich, distilled over calcium hydride under an atmosphere of argon (heptane, tributylsilane, perfluoromethylcyclohexane [PFMCH]). Tungsten hexacarbonyl used as purchased from Aldrich. All photoreactions were prepared and conducted under inert atmosphere (helium, argon or xenon as noted).

Time resolved Infrared (TRIR) Measurements

The TRIR experiments were performed either at Nottingham or at the ULTRA facility at the Rutherford Appleton Laboratory, which has been discussed in detail elsewhere^{20,21} and therefore, only a brief summary is given here. At Nottingham a 800 nm laser pulses (100 fs, 1kHz) were generated with a commercial Ti:sapphire oscillator (MaiTai) / regenerative amplifier system (Spitfire Pro/Spectra Physics, USA). The 800 nm laser beam was divided into two parts with approximately equal energy. One part pumps a TOPAS-C OPA (Light Conversion, Lithuania) to produce tunable UV-Vis-NIR pulses (300 nm - NIR) for pumping. Another part pumps a second TOPAS-C OPA with a Difference Frequency Generator (DFG) unit to produce tunable mid-IR pulses (2.5-10 μm) as a probe beam. The IR beam passes through a Ge beam splitter so that half of IR beam is reflected onto a single element MCT detector (Kolmar Technology) to serve as a reference and the other half, passing through the Ge beam splitter is focused and overlaps with the pump beam at the sample position. The UV-Vis pump pulse was optically delayed (up to 3 ns) by a 1 meter translation stage (LMA Actuator, Aerotech, USA), and focused onto the sample with a quartz lens. The polarization of the pump pulse was set at the magic angle (54.7°) relative to the probe pulse to recover the isotropic absorption spectrum. For a measurement with a longer time delay, a Q-switched Nd:YVO laser (ACE- 25QSPXHP/MOPA, Advanced Optical Technology, UK) was employed as a pump source which is synchronized to the Spitfire Pro amplifier. The delay between the ns pump and fs probe pulses varies from 0.5 ns to 100s μs with a pulse generator (DG535, Stanford Research System). The IR probe beam was dispersed with a spectrograph and detected with a $N_2(l)$ - cooled HgCdTe linear array detector (Infrared Associates, USA) which consists of 128 elements (1 mm high, 0.25 mm wide).

At Rutherford a Ti:sapphire laser amplifier (Thales Laser) produces 800 nm laser pulses (0.8 mJ, 10 kHz with a pulsewidth of 50 fs). This laser output is split and one portion is used to generate the 267 nm pump beam by harmonic generation. The second portion is sent through an optical parametric amplifier (Light Conversion) and a difference frequency generator to produce a tunable mid-IR probe. The diameter of the pump and probe beams were around 150 and 80 μm , respectively. After transmission through the sample, the IR probe is dispersed onto two linear 128 element MCT detector arrays (Infrared Associates). By the use of a chopper, the pump-on and pump-off infrared intensities can be measured and difference spectra generated. A small portion of the IR probe beam is taken before the sample and dispersed onto a 64 element MCT detector array (Infrared Associates) to provide a reference signal for beam intensity fluctuations. In both experimental set-ups, sample solution flows through a Harrick cell which was mounted on a motorized cell mount moving in x and y dimensions rapidly and continuously in a plane perpendicular to the beam direction along the z-axis.

Pump-probe X-ray Absorption Spectroscopy

Time-Resolved X-ray Absorption Spectroscopy measurements were performed at the W L_{III} edge in total fluorescence mode at beamline 11-ID-D of the Advanced Photon Source, Argonne National Laboratory. The laser pump pulse was the fourth harmonic output of a Ti:sapphire regenerative amplified laser with a 10 kHz repetition rate, giving 266nm laser pulses with 500 fs full width at half-maximum. The experiment was carried out in the standard operating mode with 24 bunches separated by 153 ns. A 3 mM solution of $\text{W}(\text{CO})_6$ was pumped through a stainless-steel tube to create a 600 μm diameter free jet. Two avalanche photodiodes (APDs) positioned at 90° on both sides of the incident X-ray beam collected the X-ray fluorescence signals. A Soller slit and an additional Cu filter inserted between the sample fluid jet and the APD detectors to block the scattering background. The outputs of the APDs were sent to a fast analyzer card (Agilent) triggered by a 10 kHz signal that was synchronized with the laser pulse. The card digitized the X-ray fluorescence signals as a function of time at 1 ns per point after each trigger and averaged repeated measurements using 4 s integration time. The fluorescence from the synchronized X-ray pulse at chosen delays after the laser excitation was used for creating the excited-state spectrum. The ground-state spectrum was obtained by averaging X-ray pulses in the previous 15 μs before the laser pulse. The synchronization between the laser and X-ray was achieved using a fast diode (“sample diode”) with a 40 ps rise time positioned where the X-ray and laser spatially overlap. The excited-state difference X-ray spectrum was created by taking the difference of the before laser spectra and excited state spectra, producing a difference spectra every 153 ns. These time points were averaged up for the analysis. Difference data were

averaged up from 153 ns time points to give good signal-to-noise. All data processed using the Athena and Artemis software suite (IFEFFIT 1.2.111).¹⁹ Detailed methodology for the EXAFS fitting the data are provided in the SI.

Results and discussion

TRIR Characterisation of $W(CO)_5(\text{heptane})$ and $W(CO)_5(\text{silane})$

Experiments on the photolysis of $W(CO)_6$ in heptane have been performed in the presence and absence of silane dopant ($HSiBu_3$), thereby allowing the formation of the W-alkane complex and subsequent substitution to the W-silane complex to be monitored. The formation of $W(CO)_5(\text{heptane})$ and reaction with $HSiBu_3$ has been previously monitored by fast time-resolved IR spectroscopy (TRIR),²² a useful technique for characterising reaction intermediates and monitoring reaction kinetics particularly of metal carbonyls.²³ These experiments served as the pre-cursor to the pump-probe XAS experiments conducted at the Advanced Photon Source, 11-ID-D to collect W L_{III} XAFS on these tungsten complexes. The TRIR spectrum obtained 1 ns after photolysis of $W(CO)_6$ in the presence of $HSiBu_3$ shows depletion of the parent $W(CO)_6$ and the formation two new bands (1958 and 1933 cm^{-1}) readily assigned to $W(CO)_5(\text{heptane})$. These bands are rapidly decay to form two new $\nu(\text{CO})$ bands (1951 and 1936 cm^{-1}) due to the formation of a W-silane complex as is evident in the TRIR spectrum obtained $50\text{ }\mu\text{s}$ after photolysis, Figure 1.

Insert Figure 1

Monitoring Photoactivation of $W(CO)_6$ in heptane at 266 nm Using XAFS.

We have repeated the TRIR experiments using the pump-probe XAS experimental setup at the 11-ID-D beam line at the Advanced Photon Source, Chicago. The photolysis reactions were monitored by pump-probe difference X-ray absorption spectroscopy (XAS) at the W L_{III} absorption edge, taking spectra collected after the laser pulse and subtracting the spectral data averaged $15\text{ }\mu\text{s}$ before laser pulse. Figure 2 shows the ground state spectrum of unreacted $W(CO)_6$, taken as the 'before' laser pulse and the spectrum taken $1\text{-}30\text{ }\mu\text{s}$ after photolysis of $W(CO)_6$ in *n*-heptane, and $50\text{-}75\text{ }\mu\text{s}$ in the presence of silane dopant.

Figure 2 also shows the difference XAS spectra derived from these spectra. The EXAFS of the difference spectrum was obtained by normalising against the post edge background with Figure 3 displaying the Fourier transform and extracted EXAFS for the photolysis of $W(CO)_6$ in heptane illustrating in k-space the backscattering of neighbouring atoms. Data were collected to ~ 10.5 keV, providing sufficient signal-to-noise to analyse the extended X-ray absorption fine structure (EXAFS) part of each spectrum, further discussed below (details of the difference fitting methodology are discussed in the SI).

Insert Figures 2 & 3

The derived difference XANES spectra for photolysis of $W(CO)_6$ in heptane, with and without the $HSiBu_3$ dopant, are given in the supporting information (Fig. S1 & S3). These data display a bleaching of the original absorption edge, that is an overall decrease in the difference absorption signal. For all pump-probe XAS reactions presented, a low energy shift of the absorption edge was observed after laser irradiation, seen as a broad positive peak at ~ 10.206 keV in the resultant difference spectra. In the reactions using more electron dense donor atoms (Si) we observe a change more akin to a line broadening effect. The red shift is still prevalent but we also observe a positive peak at ~ 10.218 keV, on the other side of the bleached absorption edge, suggesting a broadening of the absorption edge. When only the solvent is coordinated (i.e. heptane), a positive peak is not observed at 10.218 keV in the difference spectrum. The red shift suggests higher electron density on the tungsten after laser irradiation, consistent with decreased back bonding of the tungsten with the loss of a CO ligand. The line broadening suggests a lower symmetry with a larger donor atoms being closer to the tungsten atom, disrupting the remaining CO ligands far greater than H/C atoms.

Before photolysis, the XAFS spectrum of $W(CO)_6$ was analysed (Fig. S8, table 1/2 – laser off paths) affording the solution state the W-C (2.07 ± 0.02 Å) and W-O (3.21 ± 0.03 Å) which compares well to the crystallographically determined XRD values of W-C (2.02 Å) and W-O (3.18 Å) and those derived from DFT (W-C = 2.07 Å and W-O = 3.21 Å). Photolysis of $W(CO)_6$ solely in heptane without the presence of dopants produced a difference signal with reliable oscillations into the EXAFS region to ca. 8 \AA^{-1} with the EXAFS analysis of the data collected over the first 30 μ s, Figure 3, Table 1, Fig. S1 and Table S1.

The fitting method of the EXAFS is described in detail in the SI. Errors obtained from the time-resolved XAFS measures are given as standard deviations in the distances to W obtained from fitting. In essence, the method works by using the well-established EXAFS analysis software, Artemis.¹⁹ For the analysis of difference EXAFS data using this software the ground state EXAFS spectrum $W(CO)_6$ is a set parameter. The

photoproduct can then be modelled using the standard method for XAS data modelling using normal software functions to produce a theoretical EXAFS spectrum. The software is setup to subtract the ground state spectrum from the modelled photoproduct (which is derived using a range of variable parameters i.e. bond distances), resulting in the subsequent 'modelled' difference spectrum. This is then overlaid with the experimental difference EXAFS where the software can provide an accurate statistical analysis as an R-factor (described in the SI). Therefore the accuracy of the fitted difference spectrum is dictated by ensuring that the correct model of the photoproduct, as the ground state structure is known (and taken from the experimental data).

In general, the fitting analysis and the subsequent structures provided through the XAS data analysis have been strongly guided by the W-C-O bond lengths, set as variable parameters (indicated in all given XAS fitting analysis with a standard deviation provided in brackets). This allows the software to refine key parameters, such as bond distances. The output is the best statistical fit of theoretical difference with the experimental difference data refined by the software. The fit is defined by a set of fitting parameters including bond lengths from which the theoretical fit is made (using the EXAFS equation). Most importantly these parameters must also provide a sensible chemical interpretation. This chemical interpretation was guided by sensible values relating to the W-C-O bonds, a major part of all modelled spectra. Furthermore, the data analysis has used the DFT analysis as a guide. Several models have been tested during this analysis to confirm or deny potential chemical entities.

Photolysis of $W(CO)_6$ in heptane is known^{3(a)} to produce $W(CO)_5(\text{heptane})$ and these transient EXAFS data could be fitted reliably (Figures 3 and S1; Table 1 and S1) based on $W(CO)_5(\text{heptane})$ including one shorter M-CO bond *trans* to heptane, by 0.07 Å shorter than to the 4 *cis* W-CO ligands. The W-(C alkane) distance is well within the combined van der Waals radii of W and C-H,²⁴ consistent with a weaker interaction of the alkane. This reflects the weak *trans*-influence of the alkane ligand, an effect that was also observed by XRD for $[Rh(R_2PCH_2CH_2PR_2)(\eta^2:\eta^2\text{-NBA})][BARF_4]$.¹⁰ The fit of the XAFS data for $W(CO)_5(\text{heptane})$ was separated into three shells. The first consisted of W-C from the CO ligand and the second consisting of W-O, (with W-CO multiscattering pathways), and a third consisted of W-C(heptane). The CO ligands were refined using two shells, one refining the W-C bond set as variables and the second refining the W-O and all associated multiscattering paths at the same distances. For the $W(CO)_5(\text{heptane})$ model, the two W-CO shells were fitted with one associated ΔR , indicating the change in bond length as refined by the software from the initial input value (Table S1). Due to the short k-range, independent variables were kept below the allowed number by associating the change in W-C distance (ΔR_{W-C}) to equal the change in W-O and associated multiscattering paths at the same bond lengths. We can reasonably assume that the W-C bond length (set as a variable) to

equal the change in the W-O bond length. The initial models were provided by density functional theory (DFT) derived bond lengths. Given this, we could then allow the program to entirely determine and refine the W-C(Solvent) shell, determined with separate ΔR and Debye-Waller factor (σ^2) from the W-CO parameters. For this analysis, we gain a very good fit with a statistical fitting R-factor of 0.006 (see SI for definition of R-factor). When the solvent was not included in the fitting analysis, the R-factor increased to 0.008 indicating a better fit when the solvent is included.

Insert Figure 4

The structure of $W(CO)_5(\text{heptane})$ has been calculated by DFT and the binding to C1 and C2 are shown in Figure 4 and the calculation details are provided in the Table 1 and ESI. The DFT calculated *trans* and *cis* W-CO distances for C1 and C2 binding (1.96, 2.06 Å respectively) agree closely with those derived from the EXAFS analysis. The linkage to the heptane through a W-H-C bridge afforded W-C separations of 2.86 and 3.12 Å for the C1- and C2- isomer respectively (Figure 4(a) and (b)). In solution it is expected that alkanes bind via both the primary and secondary C-H bonds and there is a dynamic process with the $W(CO)_5$ moiety walking along the alkane.^{6(b)} A statistical average of the W-C distances from the calculations gives a calculated distance of 3.02 Å which is again in good agreement with the distances derived from EXAFS analysis.

Table 1 Refined distances and coordination numbers of proposed $W(CO)_5(\text{heptane})$ from the analysis of $W L_{III}$ edge EXAFS of $W(CO)_6$ in heptane over the first 30 μs after laser flash, fitted in R space (detailed fitting in ESI Table S1). ^aDFT results from coordination of primary C-H bonds to W; ^bDFT results from coordination of secondary C-H bonds to W; ^cstatistical average of primary and secondary alkane complexes calculated. [†]Determined with the same ΔR parameter as W-C(CO).

Paths	EXAFS R (Å)	DFT R(Å) ^a	DFT R(Å) ^b	DFT R(Å) ^c
<i>trans</i> W-C	1.94(1)	1.96	1.96	1.96
<i>trans</i> W-O	3.13(1) [†]	3.11	3.11	3.11
4 <i>cis</i> W-C	2.03(1)	2.06	2.06	2.06
4 <i>cis</i> W-O	3.21(1) [†]	3.20	3.20	3.20
W-C (heptane)	3.07(6)	2.86	3.12	3.02

Photoactivation of W(CO)₆ + HSiBu₃ in heptane.

Photolysis of W(CO)₆ in heptane in the presence of HSiBu₃ also gave good signal-to-noise to provide EXAFS analysis out to 8 Å⁻¹, see Figure 5 Table 2 and Table S2. These data were analysed over 50–75 μs time period after the laser pulse to ensure full conversion to the W(CO)₅(HSiBu₃) had occurred, as indicated by the TRIR data. The difference XANES signal is given in Fig. S1, where we observe a positive peak at 10.218 keV as well as a positive peak at before the bleached edge, indicating a broadening of the absorption edge, where the undoped reaction only shows a shift of the edge to low energy absorption signal.

Insert Figure 5

Table 2 Refined distances and coordination numbers of proposed W(CO)₅(HSiBu₃) from the analysis of W L_{III} edge EXAFS of W(CO)₆ + HSiBu₃ in heptane over the first 50-75 μs after laser flash, fitted in R space (detailed fitting in ESI Table S2). †Determined with the same ΔR parameter as W-C(CO). The averages of the different calculated cis environments are denoted using an asterisk.

Ligand	Paths	EXAFS R (Å)	DFT R (Å)
<i>trans</i> W-CO	W-C	2.01(1)	1.99
	W-O	3.18(1) [†]	3.14
4 <i>cis</i> W-CO	W-C	2.06(1)	2.06*
	W-O	3.23(1) [†]	3.20*
W-HSiBu ₃	W-Si	3.20(3)	3.13

The EXAFS analysis of the photolysis of W(CO)₆ + HSiBu₃ in heptane over 50-75 μs (Fig. 5 and S1; tables 2 and S2) is consistent with the TRIR results in indicating that W(CO)₅(HSiBu₃) is formed after loss of the CO ligand by the laser pulse at 266 nm in heptane doped with HSiBu₃. The W-CO shells were fitted in the same manner as the W(CO)₅(heptane) model, in this case a shorter W-CO distance was refined and the W-Si shell can be fitted with independent variables of distance (ΔR) and Debye-Waller (σ²), giving an accurate W-Si bond length of 3.20(3) Å. When attempting to fit these data without including this W-Si shell, the R-factor of the fit increased from 0.024 to 0.4, indicating that the W-Si is a very significant contribution to the fit. DFT calculations again afforded similar values (W-C *trans* 1.99, *cis*, 2.06 Å) to those derived for EXAFS analyses (Table 2). Additionally, the resolved XAS W-Si distance is in good agreement with the DFT derived distance of W-Si. Reliable kinetic information can be obtained using linear combination analysis (LCA) of XANES data, as previously reported in the literature.²⁵ Using similar methodology in our analyses, the LCA analysis gives a clear indication that there is conversion from the heptane to the silane over the first 20 μs

after the laser pulse. This is mainly dominated by a positive shift in the X-ray absorption difference signal moving from the W-heptane through to the W-Si complex. The XANES kinetic trace can be directly compared to those obtained from the TRIR data and we find excellent agreement with between these approaches with conversion between the heptane to silane bound complex occurring over the first 20 μ s when the same concentration (0.05 M) of HSiBu₃ dopant was used, Figure 2(d).

Time-resolved IR of W(CO)₆ in perfluoromethylcyclohexane (PFMCH) with and without added Xe

We have also investigated the photolysis of W(CO)₆ in the fluorinated solvent, perfluoromethylcyclohexane (PFMCH), under xenon and helium atmospheres. PFMCH is known^{4(a)} to have a particularly weak-coordination to the W(CO)₅ and could potentially be displaced by xenon. This provides a pathway to accurately characterise a very reactive and short-lived W(CO)₅L short-lived intermediate, such as organometallic noble gas complexes in solution at room temperature, through an EXAFS analysis. The generation of W(CO)₅Xe through photolysis of W(CO)₆ has previously used high-pressure liquid or supercritical Xe solutions.²⁶ The potential of using perfluoroalkanes for the generation of metal-xenon organometallics in solution by referring to early experiments using UV/Visible flash photolysis studies on Cr(CO)₆ which demonstrated the perfluoroalkanes form far less stable complexes than the corresponding non-fluorinated alkane complex.^{4(a)} Doping alkanes into perfluoroalkane solvent led to the preferential formation of the non-fluorinated alkane complex. We have previously found^{23(b)} in solution that M-Xe complexes are only ca. x2 more reactive than the corresponding metal-alkane complex.

Insert Figure 6

The TRIR spectrum obtained following photolysis (266 nm) of W(CO)₆ in PFMCH clearly shows the bleach of the parent and the production of transient bands at 1966 and 1930 cm^{-1} indicative of formation of the W(CO)₅ moiety. However, these bands are not stable and decay ($\tau = 6.4 (\pm 0.4)$ ns) to form a new transient bands at 1962 and 1935 cm^{-1} , Figure 6. The initial transient is assigned to either naked W(CO)₅ or W(CO)₅ weakly coordinated to the solvent that forms within the first 5-10 ns to the more stable solvated adduct, W(CO)₅(perfluoromethylcyclohexane); this subsequently decays on the tens of microsecond timescale. Further evidence for this assignment is given by repeating the experiments using Cr(CO)₆ as the UV/visible spectrum Cr(CO)₅X is very sensitive to the nature of X. Cr(CO)₆ was not chosen in these XAFS studies because the shorter lifetime of the first row alkane, Xe and silane species and the Cr K edge is a relatively low energy which would lead to additional experimental issues with the time-resolved XAFS measurements.

Nevertheless, TRIR experiments on $\text{Cr}(\text{CO})_6$ in PFMCH showed an initially-formed transient species in the UV/visible spectra with one set of transient IR bands (1967 and 1936 cm^{-1} ; 610 nm). UV spectroscopy demonstrated a secondary photoproduct (1962 and 1937 cm^{-1} ; 500 nm), with IR bands that are shifted. The band in the UV/visible spectrum can be compared to those obtained in low temperature matrices¹ for $\text{Cr}(\text{CO})_5\text{Ne}$ (624 nm), $\text{Cr}(\text{CO})_5(\text{CH}_4)$ (489 nm) and $\text{Cr}(\text{CO})_5(\text{CF}_4)$ (547 nm) and the experimental results obtained here support the assignment made in the tungsten experiments.

Similarly, photolysis of $\text{W}(\text{CO})_6$ in PFMCH doped with Xe (1 atm) could be followed both by IR and UV/Visible spectroscopy. The TRIR spectrum obtained 10 ns following photolysis of $\text{W}(\text{CO})_6$ in the presence of Xe shows the formation of two bands at 1963 and 1937 cm^{-1} which is again indicative of a substituted $\text{W}(\text{CO})_5$ species. However, there is a shift in the band position relative to the experiment carried out in pure PFMCH in the absence of xenon. In the presence of Xe the lifetime of the $\text{W}(\text{CO})_5$ species is extended and these results are interpreted as indicating that $\text{W}(\text{CO})_5$ preferentially coordinates Xe in the PFMCH solvent i.e. forming $\text{W}(\text{CO})_5\text{Xe}$. We can provide further evidence for this by examining the analogous reactivity of $\text{Cr}(\text{CO})_6$ in PFMCH in the presence of Xe where we form a transient species characterised with IR bands at 1966 and 1939 cm^{-1} and a UV/visible band at 490 nm . This differs from the experiments carried out in pure PFMCH and matches the previously reported positions for $\text{Cr}(\text{CO})_5\text{Xe}$ in low temperature matrices.¹ These results indicate that we can indeed form W-Xe complex in solution at room temperature. We have provided further evidence for coordination of Xe to the metal centre by photochemically generating the $\text{W}(\text{CO})_5$ moiety in PFMCH in the presence and absence of Xe using different precursors namely $\text{W}(\text{CO})_5(\text{py})$, $\text{W}(\text{CO})_5(4\text{-Acpy})$, $\text{W}(\text{CO})_5(\text{pip})$, (py = pyridine, 4-Acpy = 4-acetylpyridine and pip = piperidine) all of which lose the non-carbonyl ligand on photolysis. In each case we see spectral and lifetime changes consistent with formation of the same $\text{W}(\text{CO})_5\text{Xe}$ in PFMCH. In order to examine the binding of Xe to the metal we have performed the time-resolved XAFS experiments in PFMCH in the presence of either He (even more weakly binding) or Xe.

2.1 Time-resolved XAFS of $\text{W}(\text{CO})_6$ in perfluoromethylcyclohexane (PFMCH) with and without added Xe

A comparison of the photolysis at the W L_{III} edge by pump-probe at $8\text{ }\mu\text{s}$ after irradiation of $\text{W}(\text{CO})_6$ at 266 nm in PFMCH, for the photolysis of $\text{W}(\text{CO})_6 + \text{PFMCH}$ under helium or xenon atmosphere, shows marked changes in the XANES region of the spectra (Fig. S5 in ESI), suggesting two different photoproducts are formed. The photolysis under xenon gives a relatively higher difference absorption signal at 10.220 KeV , similar to that observed in the XANES of W-silane rather than the W-alkane complex suggesting a broadening of the absorption edge by high electron density donor atoms. Figure 7 compares the W L_{III} difference XANES data of the photoreaction under Xe and He in PFMCH, suggesting a slower decrease in the signal intensity

under Xe than under He. A good signal-to-noise for an accurate EXAFS analysis of the difference signals was obtained by averaging data over the first 8 μs for both conditions. These experimental data and the best fit analysis are shown in Figure 8 and Table 3 for reactions conducted under xenon and Table 4 under helium atmosphere (with detailed fitting analyses in the ESI; Tables S3 and S4 for xenon and helium atmospheres respectively also Figures S2 and S5).

Insert Figures 7 & 8

Table 3 Refined distances and coordination numbers of proposed $\text{W}(\text{CO})_5(\text{Xe})$ from the analysis of L_{III} edge EXAFS of $\text{W}(\text{CO})_6 + \text{PFMCH}$ under xenon over the first 8 μs after laser flash, fitted in R space (detailed fitting in ESI Table S3).

Ligand	Paths	EXAFS R (\AA)	DFT R (\AA)
Trans W-CO	W-C	1.96(1)	1.96
	W-O	3.11(1)	3.11
4 Cis W-CO	W-C	2.06(1)	2.06
	W-O	3.20(1)	3.20
W-Xe	W-Xe	3.10(2)	3.15

Table 4 Refined distances and coordination numbers of proposed $\text{W}(\text{CO})_5(\text{PFMCH})$ from the analysis of L_{III} edge EXAFS of $\text{W}(\text{CO})_6 + \text{PFMCH}$ under helium over the first 8 μs after laser flash, fitted in R space (detailed fitting in ESI Table S4). The averages of the different calculated cis environments are denoted using an asterisk. [†]Determined with the same ΔR parameter as W-C(CO).

Ligand	Paths	EXAFS R (\AA)	DFT R (\AA)
Trans W-CO	W-C	1.97(1)	2.02
	W-O	3.12(1) [†]	3.10
4 Cis W-CO	W-C	2.05(1)	2.06*
	W-O	3.19(1) [†]	3.20*
W-PFMCH	W-F	2.65(6)	2.53

Using the same difference XAS data analysis method developed for the previous studies for monitoring the formation of the $\text{W}(\text{CO})_5(\text{heptane})$ and $\text{W}(\text{CO})_5(\text{silane})$, we could gain a statistically good fit for this photolysis of $\text{W}(\text{CO})_6$ in PFMCH under different noble gas atmospheres. Under helium, using a similar fitting analysis discussed for the $\text{W}(\text{CO})_5(\text{heptane})$ model, we observe similar W-CO bond distances to those of the reaction under xenon. A W-F shell can be included independently, signifying solvent coordination at 2.65 \AA . Here we

see a high correlation with the XAS determined bond lengths and the DFT derived values. Under a xenon atmosphere, it was possible to use a greater number of variables where the W-C and W-O bond lengths were determined with separate ΔR parameters (see supporting information Table 3 and 4). In this case a W-Xe bond can also be fitted with independent variables of ΔR and σ^2 at 3.10 Å (R-factor 0.003); exclusion of W-Xe contribution significantly increases the R-factor to 0.11. From the analysis of the experimental difference data used to determine the best fit parameters, it is possible to generate theoretical EXAFS spectra for the $W(CO)_5(PFMCH)$ and $W(CO)_5Xe$ complexes and then compare the differences between compounds, as shown in the ESI, Fig. S6. These two models show significant differences in their theoretical EXAFS spectra, clearly showing a difference between both reactions with and without the presence of xenon given these models fit the associated experimental difference data very well. This technique has demonstrated how one can generate an accurate theoretical EXAFS spectrum of very short lived intermediates using real experimental data to define the physical parameters for the theoretical spectrum. Figure S7 shows the significance of the W-Xe pathway to the $W(CO)_5Xe$ model, showing this is a significant contribution. Furthermore as an additional check, it was not possible to obtain a good fit with the $W(CO)_5Xe$ model to the experimental EXAFS data of the photo reaction of $W(CO)_6$ in PFMCH under helium, indicated by a significant rise in the R-factor from 0.017 to > 0.1. The EXAFS determined distances have been reaffirmed independently by DFT calculations for all complexes. This serves as strong evidence of the presence of the W-Xe bond ~ 3.10 Å.

The calculated *trans* and *cis* W-C distances (1.96, 2.06 Å) agree closely with those derived from the EXAFS analysis. The accuracy of DFT analysis for metal-xenon bonds has been shown in a previous complex of $[AuXe_4^{2+}][Sb_2F_{11}]^{2-}$, matching well with the reported Au-Xe crystal structure.¹¹ Our determined W-Xe bond length is 0.30 Å longer compared to Au-Xe where the report stated short bond may be due to the fact¹¹ that *"Gold is the most electronegative transition element known, in part due to the strong relativistic effect"* and may explain the large charge transfer. In another examination of the accuracy of DFT defined bond lengths a tungsten coordination compound was further investigated by calculating the W-I distance in $[W(CO)_5I]$, given that I is isoelectronic with Xe and the structure has been determined by X-ray crystallography.²⁷ We find that the calculated W-I distance (2.950 Å) is in reasonable agreement with experimental value (2.871(2) Å).

Our results demonstrate, proof of concept for a potentially flexible and multi-analytical strategy to structurally probe highly reactive species that can be used to elucidate the structure, bonding and reactivity of a number of highly reactive organometallic alkane and noble gas complexes as well other weakly coordinating ligands. We report a method to directly probe the bonding of alkanes, silanes and Xe

to metal complexes in solution. We show that time-resolved X-ray measurements can monitor chemical reactions that are relevant to catalytic reactions using well known EXAFS analysis to determine highly reactive photo products. Comparison with DFT calculations show that the measured W-heptane bond lengths are consistent with the chain-walking between coordination of primary and secondary C-H groups of the alkane in solution. The measured W-Xe bond length has been reproduced using DFT methods, proving the consistency of the link between DFT, XAS and TRIR probes.

Acknowledgements

We wish to thank EPSRC for funding to the Dynamic Structural Science (DySS) consortium at the Research Complex at Harwell (EP/ I01974X/1) and Central Laser Facility at the Rutherford Appleton Laboratory for access to the laser facilities. This research used resources of the Advanced Photon Source, a U.S. Department of Energy (DOE) Office of Science User Facility operated for the DOE Office of Science by Argonne National Laboratory under Contract No. DE-AC02-06CH11357. Time-resolved XAFS spectra were measurement at beamline 11-ID-D using general user proposal beamtime (GUP #: 48118). We would also like to thank Dr Saskia Reibe-Pal and Dr Jonathon Skelton for assistance in data processing, and Professor Martyn Poliakoff and Drs Tom Penfold and Grigory Smolentsev for valuable discussions.

Supporting Information

Detailed experimental procedures and method of XAS Difference Data Fitting.

Corresponding Author:

mike.george@nottingham.ac.uk

References

- [1] Perutz R. N.; Turner, J. J. Photochemistry of Group-6 Hexacarbonyls in Low Temperature Matrices. III. Interaction of Pentacarbonyls with Noble Gases and Other Matrices. *J. Am. Chem. Soc.*, **1975**, *97*, 4791-4800.
- [2] (a) Kubas, G. J.; Ryan, R. R.; Swanson, B. I.; Vergamini, P. J.; Wasserman, H. J. Characterization of the First Examples of Isolable Molecular Hydrogen Complexes, $M(\text{CO})_3(\text{PR}_3)_2(\text{H}_2)$ ($M = \text{Mo}, \text{W}$; $R = \text{Cy}, i\text{-Pr}$). Evidence for a Side-on Bonded H_2 Ligand. *J. Am. Chem. Soc.* **1984**, *100*, 451-452; (b) Kubas, G. J.

- Molecular Hydrogen Complexes: Coordination of a Sigma Bond to Transition Metals. *Acc. Chem. Res.* **1988**, *21*, 120-128; (c) Crabtree, R. H. Transition Metal Complexation of σ Bonds. *Angew Chem. Int. Ed.*, **1993**, *32*, 789-805; (d) Kubas, G. J. Fundamentals of H₂ Binding and Reactivity on Transition Metals Underlying Hydrogenase Function and H₂ Production and Storage. *Chem. Rev.* **2007**, *107*, 4152-4205; (e) Pandey, K. K. Reactivities of Carbonyl Sulfide (COS), Carbon Disulfide (CS₂) and Carbon Dioxide (CO₂) with Transition Metal Complexes. *Coord. Chem. Rev.*, **1995**, *140*, 37-114; (f) Corey, J. Y. Reactions of Hydrosilanes with Transition Metal Complexes and Characterization of the Products. *Chem. Rev.* **2011**, *111*, 863-1071; (g) Abdalla, J. A. B.; Aldridge, S. Coordination and Activation of E-H Bonds (E=B, Al, Ga) at Transition Metal Centers. *Adv. Organomet. Chem.*, **2015**, *63*, 1-38; (h) Crabtree, R. H. Dihydrogen Complexation. *Chem. Rev.* **2016**, *116*, 8750.
- [3] (a) Young R. D. Characterisation of Alkane σ -Complexes. *Chem. Eur. J.*, 2014, *20*, 12704-12718; (b) Hall, C.; Perutz, R. N. Transition Metal Alkane Complexes. *Chem. Rev.*, **1996**, *96*, 3125-3146; (c) Lersch, M.; Tilset, M. Mechanistic Aspects of C-H Activation by Pt Complexes. *Chem. Rev.*, **2005**, *105*, 2471-2526; (d) Jones, W. D. Isotope effects in C-H bond Activation Reactions by Transition Metals. *Acc. Chem. Res.*, **2003**, *36*, 140-146; (e) Perutz, R. N.; Sabo-Etienne, S. The σ -CAM Mechanism: σ Complexes as the Basis of σ -bond Metathesis at Late-transition-metal Centers. *Angew. Chem., Int. Ed.*, **2007**, *46*, 2578-2592; (f) Weller, A. S.; Chadwick, F. M. McKay, A. I. Transition Metal Alkane-Sigma Complexes: Synthesis, Characterization, and Reactivity. *Adv. Organomet. Chem.*, **2016**, *66*, 223-276.
- [4] (a) Bonneau, R.; Kelly, J. M. Flash Photolysis of Chromium Hexacarbonyl in Perfluorocarbon Solvents. Observation of a Highly Reactive Chromium Pentacarbonyl. *J. Am. Chem. Soc.*, **1980**, *102*, 1220-1221; (b) Hermann, H.; Grevels, F.-W.; Henne, A.; Schaffner, K. J. Flash Photolysis with Infrared Detection. The Photochemistry and Secondary Thermal Reactions of M(CO)₆ [M = Cr, Mo and W]. *J. Phys. Chem.* **1982**, *86*, 5151-5154; (c) George, M. W.; Haward, M. T.; Hamley, P. A.; Hughes, C.; Johnson, F. P. A.; Popov, V. K.; Poliakoff, M. Infrared Spectroscopic Study of the Photochemical Substitution and Oxidative Addition Reactions of (η^5 -C₅R₅)M(CO)₄ Compounds of the Group 5 Metals: Characterization of the Products of Reaction with N₂, H₂, and HSiEt_{3-x}Cl_x and the Kinetic Investigation of (η^5 -C₅R₅)M(CO)₃ Intermediates. *J. Am. Chem. Soc.*, **1993**, *115*, 2286-2299; (d) Sun, X.-Z.; Nikiforov, S. M.; Grills, D. C.; Poliakoff, M.; George, M. W. Remarkable Stability of (η^5 -C₅H₅)Re(CO)₂L (L = n-Heptane, Xe, and Kr): A Time-Resolved Infrared Spectroscopic Study of (η^5 -C₅H₅)Re(CO)₃ in Conventional and Supercritical Fluid Solution. *J. Am. Chem. Soc.*, **1997**, *119*, 7521-7525; (e) Cowan, A. J.; Portius, P.; Kawanami, H. K.; Jina, O. S.; Grills, D. C.; Sun, X.-Z.; McMaster, J.; George, M. W. Time-resolved infrared (TRIR) Study on the Formation and Reactivity of Organometallic Methane and Ethane Complexes in Room Temperature Solution. *Proc. Natl. Acad. Sci.*, **2007**, *104*, 6933-6938; (f) Besora, M.; Carreon-Macedo, J.-L.; Cowan, A. J.; George, M. W.; Harvey, J. N.; Portius, P.; Ronayne, K. L.; Sun,

- X.-Z.; Towrie, M. A Combined Theoretical and Experimental Study on the Role of Spin States in the Chemistry of Fe(CO)₅ Photoproducts. *J. Am. Chem. Soc.*, **2009**, *131*, 3583-3592.
- [5] (a) Roithova, J.; Schroeder, D. Selective Activation of Alkanes by Gas-Phase Metal Ions. *Chem. Rev.*, **2010**, *110*, 1170-1211; (b) Almelin, M.; Schlangen, M.; Schwarz, H. On the Mechanisms of Degenerate Ligand Exchange in [M(CH₃)⁺/CH₄ couples (M = Fe, Co, Ni, Ru, Rh, Pd, Os, Ir, Pt) as Explored by Mass Spectrometric and Computational Studies: Oxidative Addition/Reductive Elimination Versus σ -complex-assisted Metathesis. *Chem.-Eur. J.* **2008**, *14*, 5229-5236; (c) Schlangen, M.; Schwarz, H. Ligand and Electronic-structure Effects in Metal-mediated Gas-phase Activation of Methane: A Cold Approach to a Hot Problem. *Dalton Trans.* **2009**, *46*, 10155-10165.
- [6] (a) Geftakis, S.; Ball, G. E. Direct Observation of a Transition Metal Alkane Complex, CpRe(CO)₂(cyclopentane), using NMR spectroscopy. *J. Am. Chem. Soc.*, **1998**, *120*, 9953-9954; (b) Lawes, D. J.; Geftakis, S.; Ball, G. E. Insight into Binding of Alkanes to Transition Metals from NMR Spectroscopy of Isomeric Pentane and Isotopically Labeled Alkane Complexes. *J. Am. Chem. Soc.*, **2005**, *127*, 4134-4135; (c) Lawes, D. J.; Darwish, T. A.; Clark, T.; Harper, J. B.; Ball, G. E. A Rhenium-cyclohexane Complex with Preferential Binding of Axial C-H bonds: A Probe into the Relative Ability of C-H, C-D, and C-C bonds as Hyperconjugative electron donors? *Angew. Chem., Int. Ed.*, **2006**, *45*, 4486-4490; (d) Ball, G. E.; Brookes, C. M.; Cowan, A. J.; Darwish, T. A.; George, M. W.; Kawanami, H. K.; Portius, P. Rourke, J. P. A Delicate Balance of Complexation vs. Activation of Alkanes Interacting with [Re(Cp)(CO)(PF₃)] studied with NMR and time-resolved IR spectroscopy. *Proc. Natl. Acad. Sci.*, **2007**, *104*, 6927-6931; (e) Duckett, S. B.; George, M. W.; Jina, O. S.; Matthews, S. L.; Perutz, R. N.; Sun, X.-Z.; Vuong, K. Q. A Systematic Approach to the Generation of Long-lived Metal Alkane Complexes: Combined IR and NMR Study of (Tp)Re(CO)₂(cyclopentane). *Chem. Commun.*, **2009**, 1401-1403; (f) Bernskoetter, W. H.; Schauer, C. K.; Goldberg, K. I.; Brookhart, M. Characterization of a Rhodium(I) σ -Methane Complex in Solution. *Science*, **2009**, *326*, 553; (g) Calladine, J. A.; Torres, O.; Anstey, M.; Ball, G. E.; Bergman, R. G.; Curley, J.; Duckett, S. B.; George, M. W.; Gilson, A. I.; Lawes, D. J.; Perutz, R. N.; Sun, X.-Z.; Vollhardt, P. C. Photoinduced N₂ Loss as a Route to Long-lived Organometallic Alkane Complexes: A Time-resolved IR and NMR Study. *Chem. Sci.*, **2010**, *1*, 622-630; (h) Young, R. D.; Hill, A. F.; Hillier, W.; Ball, and G. E. Transition Metal-Alkane σ -Complexes with Oxygen Donor Co-ligands. *J. Am. Chem. Soc.*, **2011**, *133*, 13806-13809; (i) Young, R. D.; Lawes, D. J.; Hill, A. F.; Ball, G. E. Observation of a Tungsten Alkane σ -Complex Showing Selective Binding of Methyl Groups Using FTIR and NMR Spectroscopies. *J. Am. Chem. Soc.*, **2012**, *134*, 8294-8297; (j) J. A. Calladine, S. B. Duckett, M. W. George, S. L. Matthews, R. N. Perutz, O. Torres and K. Q. Vuong, Manganese Alkane Complexes: An IR and NMR Spectroscopic Investigation. *J. Am. Chem. Soc.*, **2011**, *133*, 2303-2310; (k) Torres, O.; Calladine, J. A.; Duckett, S. B.; George, M. W.; Perutz, R. N. Detection

- of σ -alkane Complexes of Manganese by NMR and IR Spectroscopy in Solution: (η^5 -C₅H₅)Mn(CO)₂(ethane) and (η^5 -C₅H₅)Mn(CO)₂(isopentane). *Chem. Sci.* **2015**, *6*, 418-424; (I) Yau, H. M.; McKay, A. I.; Hesse, H.; Xu, R.; He, M.; Holt, C. E.; Ball, G. E. Observation of Cationic Transition Metal-Alkane Complexes with Moderate Stability in Hydrofluorocarbon Solution. *J. Am. Chem. Soc.*, **2016**, *138*, 281-288.
- [7] Ball, G. E.; Darwish, T.; Geftakis, S.; George, M. W.; Lawes, D. J.; Portius, P.; Rourke, J. P. Characterization of an organometallic xenon complex using NMR and IR spectroscopy. *Proc. Nat. Acad. Sci.*, **2005**, *102*, 1853-1858
- [8] (a) Evans, D. R.; Drovetskaya, T.; Bau, R.; Reed, C. A.; Boyd, P. D. W. Heptane Coordination to an Iron(II) Porphyrin. *J. Am. Chem. Soc.*, **1997**, *119*, 3633-3649; (b) Castro-Rodriguez, I.; Nakai, H.; Gantzel, P.; Zakharov, L. N.; Rheingold, A. L.; Meyer, K. Evidence for Alkane Coordination to an Electron-Rich Uranium Center. *J. Am. Chem. Soc.*, **2003**, *125*, 15734-15735; (c) Andreychuk, N. R.; Emslie, D. J. H. Potassium-Alkane Interactions within a Rigid Hydrophobic Pocket. *Angew. Chem., Int. Ed.*, **2013**, *52*, 1696-1699.
- [9] Bloch, E. D.; Queen, W. L.; Krishna, R.; Zadrozny, J. M.; Brown, C. M.; Long, J. R. Hydrocarbon Separations in a Metal-Organic Framework with Open Iron(II) Coordination Sites *Science*, **2012**, *335*, 1606-1610.
- [10] (a) Pike, S. D.; Thompson, A. L.; Algarra, A. G.; Apperley, D. C.; Macgregor, S. A.; Weller, A. S. Synthesis and Characterization of a Rhodium(I) σ -Alkane Complex in the Solid State. *Science*, **2012**, *337*, 1648-1651; (b) Pike, S. D.; Chadwick, F. M.; Rees, N. H.; Scott, M. P.; Weller, A. S.; Krämer, T.; Macgregor, S. A. Solid-State Synthesis and Characterization of σ -Alkane Complexes, [Rh(L₂)(η^2 , η^2 -C₇H₁₂)] [BAR^F₄] (L₂ = Bidentate Chelating Phosphine). *J. Am. Chem. Soc.*, **2015**, *137*, 820-833; (c) Chadwick, F. M.; N Rees, N. H.; Weller, A. S.; Krämer, T.; Iannuzzi, M.; Macgregor, S. A. A Rhodium-Pentane σ -Alkane Complex: Characterization in the Solid State by Experimental and Computational Techniques. *Angew. Chem., Int. Ed.*, **2016**, *55*, 3677-3681; (d) McKay, A. I.; Kramer, T.; Rees, N. H.; Thompson, A. L.; Christensen, K. E.; Macgregor, S. A.; Weller, A. S. Formation of a σ -alkane Complex and a Molecular Rearrangement in the Solid-State: [Rh(Cyp₂)PCH₂CH₂PCyp₂](η^2 , η^2 -C₇H₁₂)] [BAR^F₄]. *Organometallics*, **2017**, *36*, 22-25; (e) Chadwick, F. M.; McKay, A. I.; Martinez-Martinez, A. J.; Rees, N. H.; Krämer, T.; Macgregor, S. A.; Weller, A. S. Solid-state Molecular Organometallic Chemistry. Single-crystal to Single-crystal Reactivity and Catalysis with Light Hydrocarbon Substrates. *Chem. Sci.*, **2017**, *8*, 6014-6029.
- [11] Seidel, S.; Seppelt, K. Xenon as a complex ligand: The tetra xenono gold(II) cation in AuXe₄²⁺(Sb₂F₁₁)₂ *Science* **2000**, *290*, 117-118.

- [12] (a) Lipke, M. C.; Liberman-Martin, A. L.; Tilley, T. D. Electrophilic Activation of Silicon-Hydrogen Bonds in Catalytic Hydrosilations. *Angew. Chem. Int. Ed.* **2017**, *56*, 2260-2294; (b) Corey, J. Y. Reactions of Hydrosilanes with Transition Metal Complexes. *Chem. Rev.* **2016**, *116*, 11291-1143 (c) Cheng, C.; Hartwig, J. F. Catalytic Silylation of Unactivated C-H Bonds. *Chem. Rev.* **2015**, *115*, 8946-8975; (d) Corey, J. Y. Reactions of Hydrosilanes with Transition Metal Complexes and Characterization of the Products. *Chem. Rev.* **2011**, *111*, 863-1071; (e) Alcaraz, G.; Sabo-Etienne, S. NMR: A Good Tool to Ascertain sigma-silane or sigma-borane Formulations? *Coord. Chem. Rev.* **2008**, *252*, 2395-2409; (f) Corey, J. Y.; Braddock-Wilking, J. *Chem. Rev.* **1999**, *99*, 175-292.
- [13] (a) Chergui, M.; Collet, E. Photoinduced Structural Dynamics of Molecular Systems Mapped by Time-Resolved X-ray Methods. *Chem. Rev.* **2017**, *117*, 11025-11065 and references therein; (b) Bressler, C.; Chergui, M. Ultrafast X-ray absorption spectroscopy. *Chem. Rev.* **2004**, *104*, 1781-1812 and references therein.
- [14] Gawelda, W.; Pham, V.-T.; van der Veen, R. M.; Grolimund, D.; Abela, R.; Chergui, M.; Bressler, C. Structural Analysis of Ultrafast Extended X-ray Absorption Fine Structure with Subpicometer Spatial Resolution: Application to Spin Crossover Complexes. *J. Chem. Phys.*, **2009**, *130*, 124520.
- [15] van der Veen, R. M.; Milne, C. J.; El Nahhas, A.; Lima, F. A. ; Pham, V. T.; Best, J.; Weinstein, J. A.; Borca, C. N.; Abela, R.; Bressler, C.; Chergu M. Structural Determination of a Photochemically Active Diplatinum Molecule by Time-Resolved EXAFS Spectroscopy. *M. Angew. Chem. Int. Ed.* **2009**, *48*, 2711-2714
- [16] Thiel, D. J. Livins P.; Stern, E. A.; Lewis A. Microsecond-resolved XAFS of the Triplet Excited State of $[\text{Pt}_2(\text{P}_2\text{O}_5\text{H}_2)_4]^{4-}$ *Nature*, **1993**, *362*, 40-43.
- [17] Penfold, T. J.; Szlachetko, J.; Santomauro, F. G.; Britz, A.; Gawelda, W.; Doumy, G.; March, A. M.; Southworth, S. H.; Rittmann, J.; Abela, R.; Chergui, M.; Milne, C. J. Revealing hole trapping in zinc oxide nanoparticles by time-resolved X-ray spectroscopy. *Nat. Com.* **2018**, *9*, 478.
- [18] (a) Harpham, M. R.; Stickrath, A. B.; Zhang, X. Y.; Huang, J.; W. Mara, M.; Chen, L. X.; Liu, D. J. Photodissociation Structural Dynamics of Triruthenium Dodecacarbonyl Investigated by X-ray Transient Absorption Spectroscopy. *J. Phys. Chem. A.*, **2013**, *117*, 9807-9813; (b) König, C. F. J.; van Bokhoven, J. A.; Schildhauer, T. J.; Nachtegaal, M. Quantitative Analysis of Modulated Excitation X-ray Absorption Spectra: Enhanced Precision of EXAFS Fitting. *J. Phys. Chem. C*, **2012**, *116*, 19857-19866; (c) Korobko, R.; Lerner, A.; Li, Y.; Wachtel, E.; Frenkel, A. I.; Lubomirsky, I. In-situ Extended X-ray Absorption Fine Structure Study of Electrostriction in Gd Doped Ceria. *Appl. Phys. Lett.*, **2015**, *106*, 042904; (d) Pettifer, R. F.; Mathon, O.; Pascarelli, S.; Cooke, M. D.; Gibbs, M. R. J. Measurement of Femtometre-scale Atomic Displacements by X-ray Absorption Spectroscopy. *Nature*, **2013**, *435*, 78-81.

- [19] Ravel, B.; Newville, M. ATHENA, ARTEMIS, HEPHAESTUS: data analysis for X-ray absorption spectroscopy using IFEFFIT, *J. Synchrotron Rad.* **2005**, *12*, 537-541.
- [20] Brennan, P.; George, M. W.; Jina, O. S.; Long, C.; McKenna, J.; Pryce, M. T.; Sun, X.-Z.; Vuong, K. Q. Photoinduced Se-C insertion following photolysis of $(\eta^5\text{-C}_4\text{H}_4\text{Se})\text{Cr}(\text{CO})_3$. A picosecond and nanosecond time-resolved infrared, matrix isolation, and DFT investigation *Organometallics* **2008**, *27*, 3671-3680.
- [21] Greetham, G. M.; Burgos, P.; Cao, Q.; Clark, I. P.; Codd, P. S.; Farrow, R. C.; George, M. W.; Kogimtzis, M.; Matousek, P.; Parker, A. W.; Pollard, M. R.; Robinson, D. A.; Xin, Z.-J.; Towrie, M. ULTRA: A unique instrument for time-resolved spectroscopy *Appl. Spectrosc.* **2010**, *64*, 1311-1319
- [22] (a) Snee, P. T.; Payne, C. K.; Kotz, K. T.; Yang, H.; Harris, C. B. Triplet organometallic reactivity under ambient conditions: An ultrafast UV pump/IR probe study. *J. Am. Chem. Soc.*, **2001**, *123*, 2255-2264; (b) Yang, H.; Kotz, K. T.; Asplund, M. C.; Harris, C. B. Femtosecond infrared studies of silane silicon-hydrogen bond activation. *J. Am. Chem. Soc.*, **1997**, *119*, 9564-9565.
- [23] (a) George, M. W.; Poliakoff, M.; Turner, J. J. Nanosecond Time-resolved Infrared Spectroscopy: A Comparative View of Spectrometers and their Applications in Organometallic Chemistry. *Analyst*, **1994**, *119*, 551-560; (b) Kuimova, M. K.; Alsindi, W.; Dyer, J.; Grills, D. C.; Jina, O.; Matousek, P.; Parker, A. W.; Portius, P.; Sun, X. Z.; Towrie, M.; Wilson, C.; Yang J.; George M. W. Using Picosecond and Nanosecond Time-resolved Infrared Spectroscopy for the Investigation of Excited States and Reaction Intermediates of Inorganic Systems. *J. Chem. Soc. Dalton Trans.* **2003**, 3996-4006.
- [24] Alvarez, S. A Cartography of the van der Waals Territories. *Dalton Trans.* **2013**, *42*, 8617-8636.
- [25] (a) Nelson, R. C.; Miller J. T. An introduction to X-ray Absorption Spectroscopy and its *in situ* Application to Organometallic Compounds and Homogeneous Catalysts *Catal. Sci. Technol.*, **2012**, *2*, 461-470 (b) Asakura, H.; Shishido, T.; Tanaka, T. In Situ Time-Resolved XAFS Study of the Reaction Mechanism of Bromobenzene Homocoupling Mediated by $[\text{Ni}(\text{cod})(\text{bpy})]$ *J. Phys. Chem. A*, **2012**, *116*, 4029-4034.
- [26] (a) Sun, X-Z.; George, M. W.; Kazarian, S. G.; S. M. Nikiforov; Poliakoff, M. Can organometallic noble gas compounds be observed in solution at room temperature? A time-resolved infrared (TRIR) and UV spectroscopic study of the photochemistry of $\text{M}(\text{CO})_6$ (M=Cr, Mo, and W) in supercritical noble gas and CO_2 solution. *J. Am. Chem. Soc.*, **1996**, *118*, 10525-10532; (b) Weiller, B. H.; Wasserman, E. P.; Moore, C. B.; Bergman, R. G. Organometallic CO substitution kinetics in liquid Xe by fast time-resolved IR spectroscopy *J. Am. Chem. Soc.*, **1993**, *115*, 4326-4330; (c) Weiller, B. H. Metal carbonyl complexes with xenon and krypton: IR spectra, CO substitution kinetics and bond energies *J. Am. Chem. Soc.*, **1992**, *114*, 10910-10915; (d) Simpson, M. B.; Poliakoff, M. Turner, J. J.; Maier, W. B.;

McLaughlin, J. G. $[\text{Cr}(\text{CO})_5\text{Xe}]$ in solution; the first spectroscopic evidence *J. Chem. Soc. Chem. Commun.*, **1983**, 1355-1357.

[27] Palitzsch, W.; Böhme, U.; Roewer G. $[\text{Li}(\text{dime})_2][\text{W}(\text{CO})_5\text{I}]$ as a Novel Synthone for the Preparation of Silyl, Amino and Organyl Derivatives of Pentacarbonyl Tungsten (dime=diethylene glycol dimethyl ether). *Chem Commun.* **1997**, 803-804.

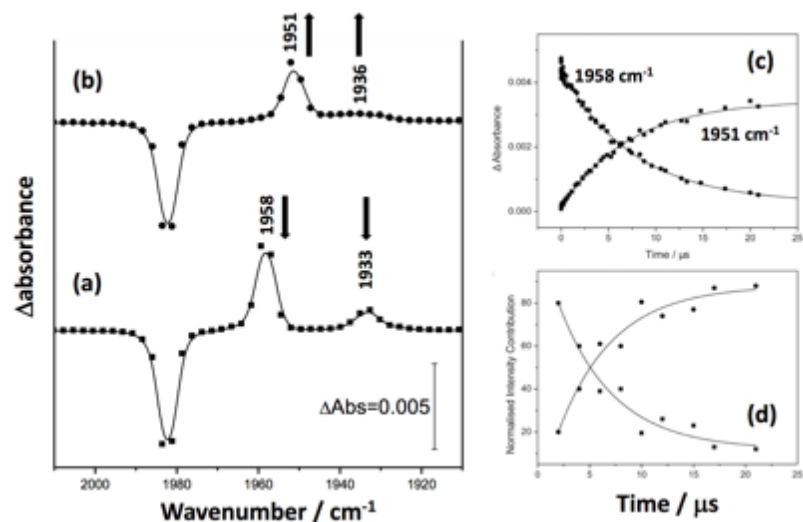


Figure 1 Time-resolved IR (TRIR) spectra obtained (a) 1 ns and (b) 50 μ s following photolysis (266 nm) of $W(CO)_6$ in *n*-heptane doped with $HSiBu_3$ (0.05 M). (c) TRIR decay traces taken at 1958 and 1951 cm^{-1} from the TRIR shown in (a) and (b). (d) Linear combination XANES fitting analysis of the photolysis of $W(CO)_6$ in the presence of $HSiBu_3$ in heptane over first 20 μ s. Using of the determined $W(CO)_5$ (heptane) (decay) and $W(CO)_5$ ($HSiBu_3$) (growth) as standards (XANES spectra shown Fig. S3).

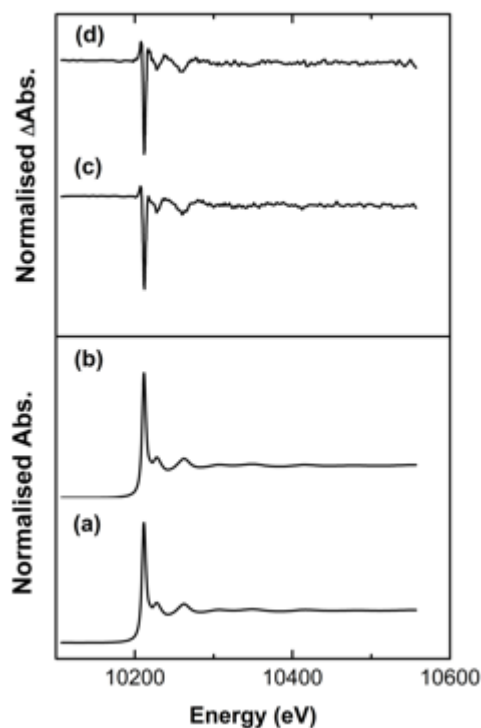


Figure 2 Displays the normalised $W_{L_{III}}$ edge XAS spectra of (a) before laser and (b) after laser excitation (across 1-30 μ s) of $W(CO)_6$ in heptane. (c) Shows the transient absorption spectrum of the $W_{L_{III}}$ edge XAS from the subtraction of the 'after' (b) and 'before' (a) laser $W_{L_{III}}$ edge spectra. (d) Shows the same derived transient absorption spectrum as (c) with $HSiBu_3$ (0.05 M) added to the heptane solvent, at 50 - 75 μ s after photolysis.

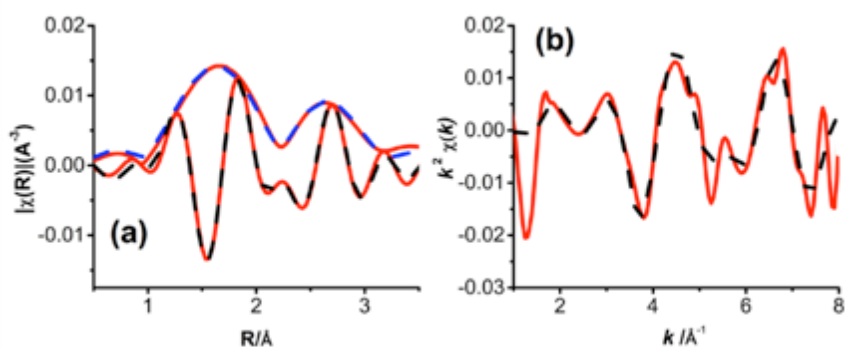


Figure 3 Displaying the W L_{III} edge difference extracted EXAFS (Red) and fitting analysis (Dashed) of $W(CO)_6$ in heptane 0-30 μs after the laser pulse. (a) Shows the k^2 -weighted Fourier transform (red lines represent experimental data including modulated imaginary part with the fit analysis as blue dashed line and black dashed line as the imaginary part) EXAFS and (b) k^2 -weighted extracted EXAFS spectrum with black dashed line as the fit analysis (a smoothing function has been applied, detailed in the SI).

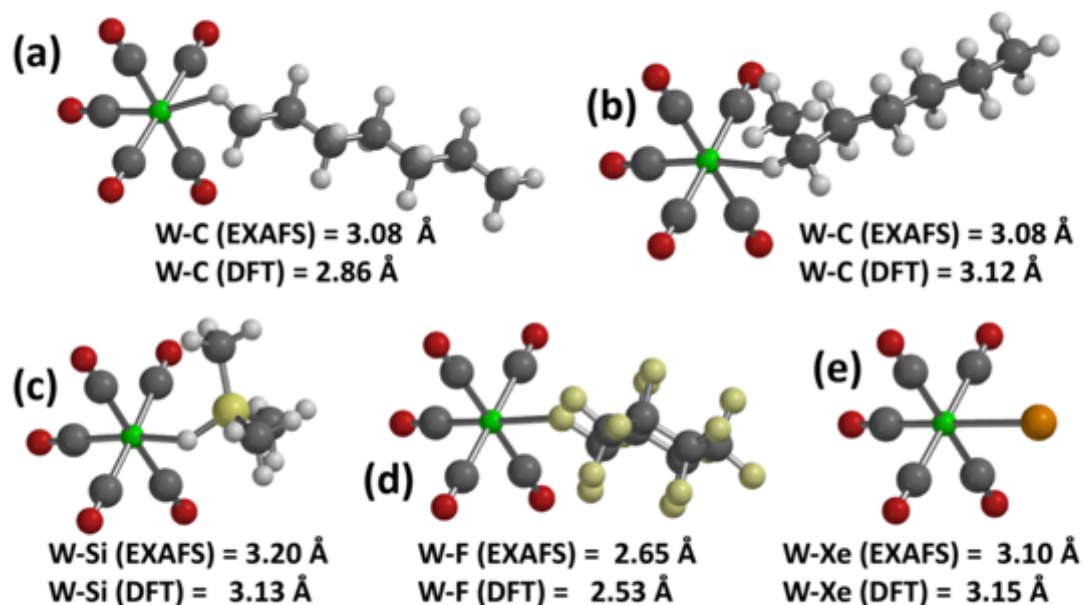


Figure 4: Showing DFT calculated structure with the key distances derived from the DFT calculations and from fitting the XAFS data for the binding mode of (a) $W(CO)_5$ (heptane) with the alkane binding via primary C-H; (b) $W(CO)_5$ (heptane) with the alkane binding via secondary C-H; (c) $W(CO)_5(HSiBu_3)$; (d) $W(CO)_5$ (perfluoro-methylcyclohexane) and (e) $W(CO)_5Xe$. Note for (a) and (b) that the DFT predicts significant differences between the primary and secondary alkane structures while the EXAFS experiment only provides a single measurement. The relationship between the DFT and EXAFS is discussed within the text.

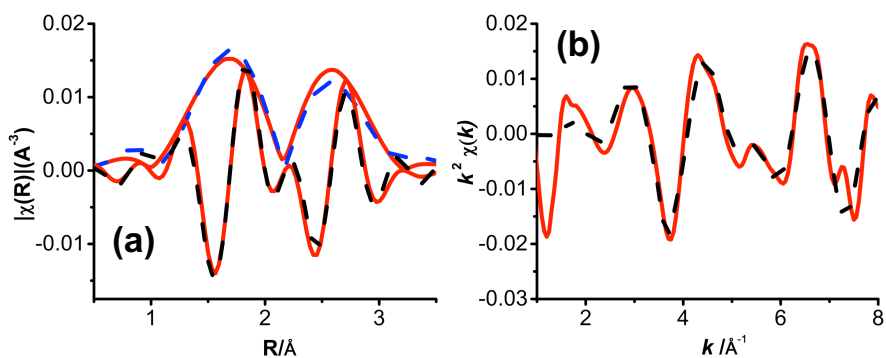


Figure 5 Displaying the W L_{III} edge difference extracted EXAFS (Red) and fitting analysis (Dashed) of $W(CO)_6 + HSiBu_3$ in heptane 50-75 μs (i.e. an average over this 25 μs interval) after the laser pulse. (a) Shows the k^2 -weighted Fourier transform (red lines represent experimental data including modulated imaginary part with the fit analysis as blue dashed line and black dashed line as the imaginary part) EXAFS and (b) k^2 -weighted extracted EXAFS spectrum with black dashed line as the fit analysis (a smoothing function has been applied, detailed in the SI).

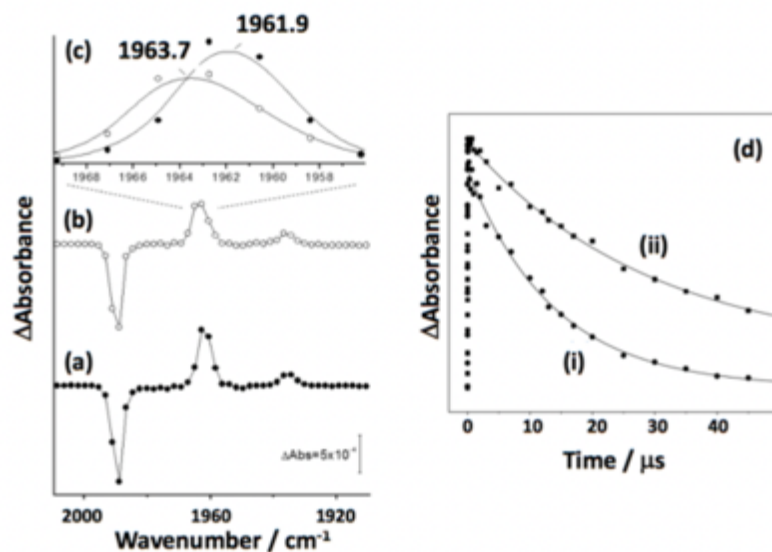


Figure 6 TRIR spectra obtained 10 ns after photolysis (355 nm) of $W(CO)_6$ in (a) PFMCH and (b) PFMCH doped with Xe. (c) Presents an expanded region of the TRIR from these spectra in pure PFMCH (\bullet) and PFMCH doped with Xe (\circ) and (d) shows the TRIR kinetic traces obtained at the band maximum in (i) in pure PFMCH and (ii) PFMCH doped with Xe (1 atm).

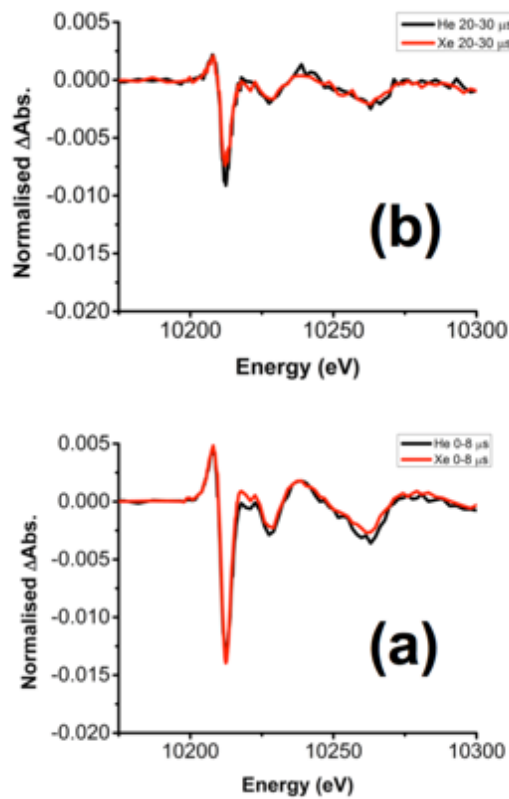


Figure 7 Time interval Displaying the W L_{III} edge transient absorption difference spectra of the two reaction conditions; under helium (Black) and under xenon (Red), displaying two time points at (a) 0 – 8 μs and (b) 20 – 30 μs.

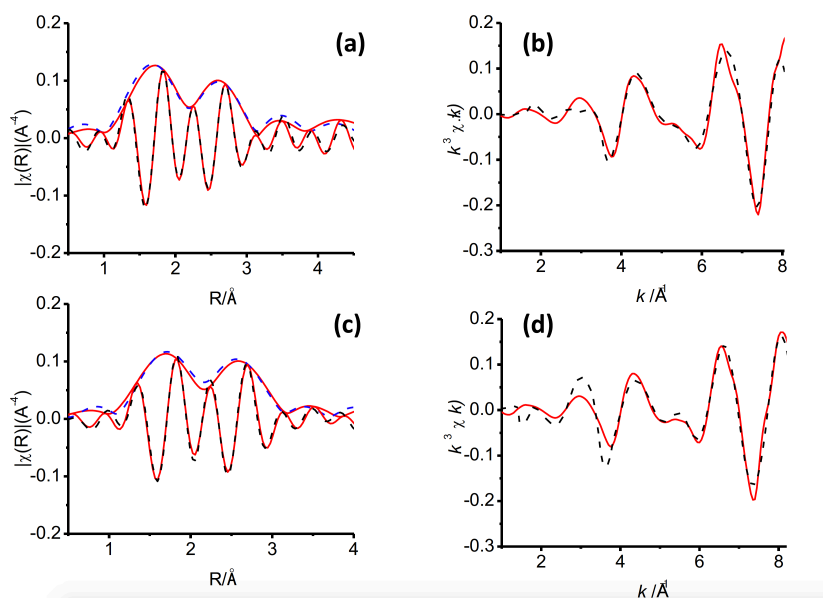


Figure 8 Displaying the W L_{III} edge difference extracted EXAFS (Red) and fitting analysis (Dashed) of: (a) the k^3 -weighted Fourier transform (red lines represent experimental data including modulated imaginary part with the fit analysis as blue dashed line and black dashed line as the imaginary part) of $W(CO)_6 + PFMCH$ under xenon atmosphere over the first 8 μs and (b), associated k^3 -weighted extracted EXAFS spectrum with black dashed line as the fit analysis. (c) The k^3 -weighted Fourier transform (red lines represent experimental data including modulated imaginary part with the fit analysis as blue dashed line and black dashed line as the imaginary part) of $W(CO)_6 + PFMCH$ under helium atmosphere over the first 8 μs and (d), associated k^3 -weighted extracted EXAFS spectrum with black dashed line as the fit analysis (a smoothing function has been applied, detailed in the SI).

Monitoring the Formation and Reactivity of Organometallic Alkane and Fluoroalkane Complexes with Silanes and Xe Using Time-resolved XAFS

Stuart A. Bartlett^{1,2,3}, Nicholas A. Besley,⁴ Andrew J. Dent,⁵ Sofia Diaz-Moreno,⁵ John Evans,^{1,5,6} Michelle L. Hamilton^{1,4}, Magnus W. D. Hanson-Heine,⁴ Raphael Horvath,⁴ Valentina Manici,^{1,4} Xue-Zhong Sun,⁴ Michael Towrie,^{1,7} Lingjun Wu,⁴ Xiaoyi Zhang⁸ and Michael W. George,^{1,4,9}

¹DySS, Research Complex at Harwell, Rutherford Appleton Laboratory, Didcot, OX11 0FA, UK

²School of Chemistry, The University of Sydney, Eastern Ave, Sydney NSW 2006, Australia

³Department of Chemistry, University of Bath, Claverton Down, Bath, BA2 7AY, United Kingdom

⁴School of Chemistry, University of Nottingham, University Park NG7 2RD, United Kingdom

⁵Diamond Light Source, Rutherford Appleton Laboratory, Didcot, OX11 0DE, United Kingdom

⁶Chemistry, University of Southampton, Southampton, SO17 1BJ, UK.

⁷Central Laser Facility, Research Complex at Harwell, Rutherford Appleton Laboratory, Chilton, Oxfordshire OX11 0QX, United Kingdom

⁸X-ray Science Division, Argonne National Laboratory, Argonne, USA

⁹Department of Chemical and Environmental Engineering, University of Nottingham Ningbo China, 199 Taikang East Road, Ningbo 315100, China

Computational Details

Density functional theory calculations were used to calculate minimum energy geometries and to simulate harmonic vibrational frequencies using the M06 exchange-correlation functional^{S1} within the Q-Chem software package.^{S2} Calculations were converged using the 6-311++G(d,p) basis set for C, O, Si, F, and H atoms, and the LANL08 pseudo-potential and basis set for W and Xe.^{S3} The EML-(128,590) integration grid was used with this functional and detailed discussions of integration grids can be found elsewhere.^{S4-S6} Optimized geometries were confirmed by the absence of imaginary frequencies and the harmonic frequencies were scaled by a uniform factor of 0.96 to account for anharmonic effects.^{S7}

Method of XAS Difference Data Fitting

Using Feff software (Athena and Artemis) it is possible to derive EXAFS parameters from difference spectrum (such as Debye-Waller factors [σ^2] and path lengths [ΔR]) with a statistical validation.

This first requires a standard EXAFS fitting analysis of the ground state spectrum used to generate the difference spectrum. Then when performing the fitting analysis of the difference spectrum, the pre-

determined ground state parameters can be applied to the fit as a fixed parameters, where the amplitude factor is set to be equal to the negative of the difference data under analysis. Thus setting up equation (1) in the software.

This allows whole structures models of the photoexcited state/product to be input into the software in usual circumstances. When the difference data is fit, the software performs the difference subtraction in situ of the two models to give a statistical fit analysis of the difference spectrum:

$$\Delta\chi = \chi_{\text{Lon}} - \chi_{\text{Loff}} \quad (1)$$

Where $\Delta\chi$ is the fitted difference data, χ_{Lon} in the modelled photoexcited state/product, and $-\chi_{\text{Loff}}$ is the predetermined ground state. This follows a previously published article using a theoretical basis to determine physical parameters using difference EXAFS data. S8 [4]

Thus by obtaining the best fit analysis of $\Delta\chi$ through refining the model of χ_{Lon} , we can use the Artemis software to plot that model to provide a theoretical EXAFS spectrum of that complex, using the experimental difference data.

- **Amplitude reduction factor – S_0^2 .**

Thus, the amplitude reduction factor of the laser off can be reasonably assumed to equal the negative of the laser on (on the assumption all reacted ground state forms the photoexcited state/product). Therefore, any unreacted $W(\text{CO})_6$ is removed through the difference method, leaving only the photoactivated species minus the original $W(\text{CO})_6$ from which the photoproduct originated in the before laser spectrum. Therefore the resulting value of the S_0^2 factor is a representation of the $W(\text{CO})_6$ conversion.

Determination of the measure of the accuracy of fitting, R-factor

The statistical fitting analysis follows the IFEFFET software and further detail is provided in the published literature.^{S9} Essentially, a difference function, f , between the data and calculation is computed for each data point included in the evaluation of the fit, where the fit is derived from the sum of the pathways given by the EXAFS equation. The overall statistical verification of the fit as compared with the data is evaluated in the R-space, given by R_{fac} . R_{fac} is evaluated over all data points included in the fit (as defined by the R value given for each analysis). It is interpreted as a numerical evaluation of how closely the fitted function over plots the data. i.e. the smaller the R_{fac} the better the fit. As such it is a useful metric for judging accuracy of the data and the model. It does not define the physical viability of the individual parameters contributing to the fit and thus both R_{fac} and all parameters contributing to that fit must be judged accordingly. The definition of the R_{fac} for the EXAFS analysis is:

$$R_{\text{fac}} = \frac{\sum_{i=1}^N [f(R_i)]^2}{\sum_{i=1}^N \left([\text{Re}(\tilde{\chi}(R_i|\text{data}))]^2 + [\text{Im}(\tilde{\chi}(R_i|\text{data}))]^2 \right)}$$

Where $f(R_i) = \text{Re}[\tilde{\chi}(R_i|\text{data}) - \tilde{\chi}(R_i|\text{theory})] + \text{Im}[\tilde{\chi}(R_i|\text{data}) - \tilde{\chi}(R_i|\text{theory})]$

Where Re = Real Fourier transform, Im = Imaginary Fourier transform,

$\tilde{\chi}$ = Fourier Transform EXAFS (determined by the k -range); f = difference between the data and calculation for each data point included in the evaluation of the fit.

For a fit evaluated in the R-space, the difference function includes the real and imaginary parts of the Fourier transformed data as given above by $f(R_i)$ (as such imaginary part and [Imaginary + real FT] are shown in each fitting analysis).

XAS analysis, parameters and data.

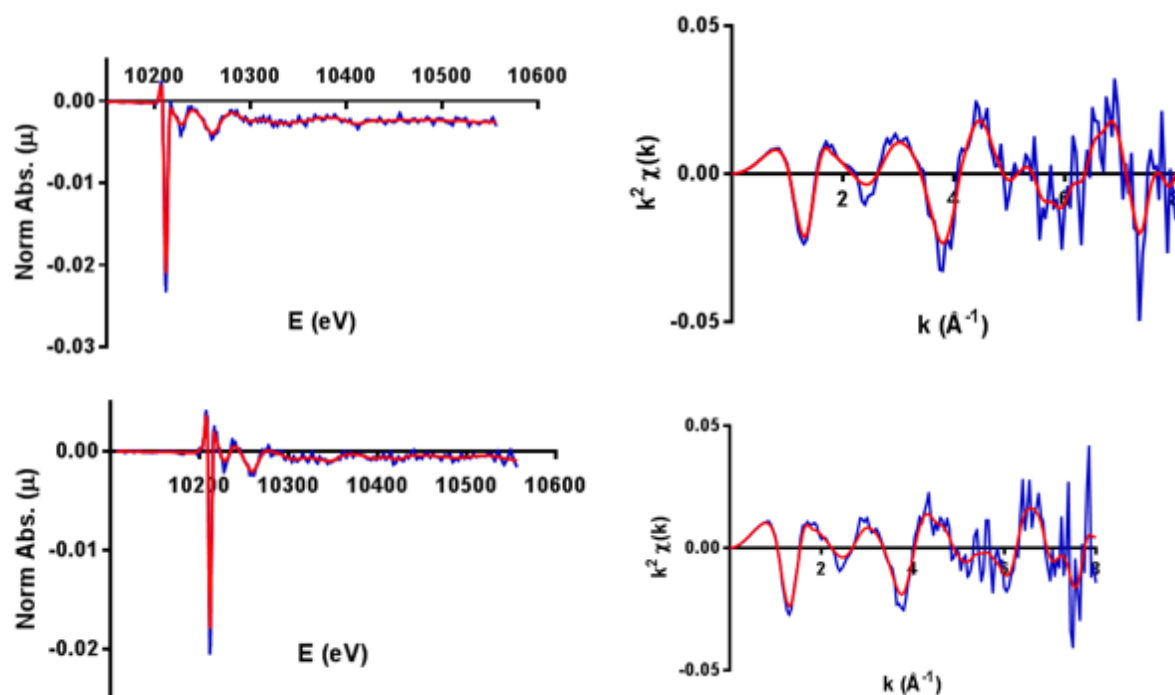


Figure S1 Displaying real and interpolative smoothed data (normalised absorption and EXAFS) of (Top) W(CO)₆ + Heptane and (Bottom) W(CO)₆ + HSiBu₃. Interpolation was used for the EXAFS analysis and for the linear combination analysis of the heptane-silane conversion.

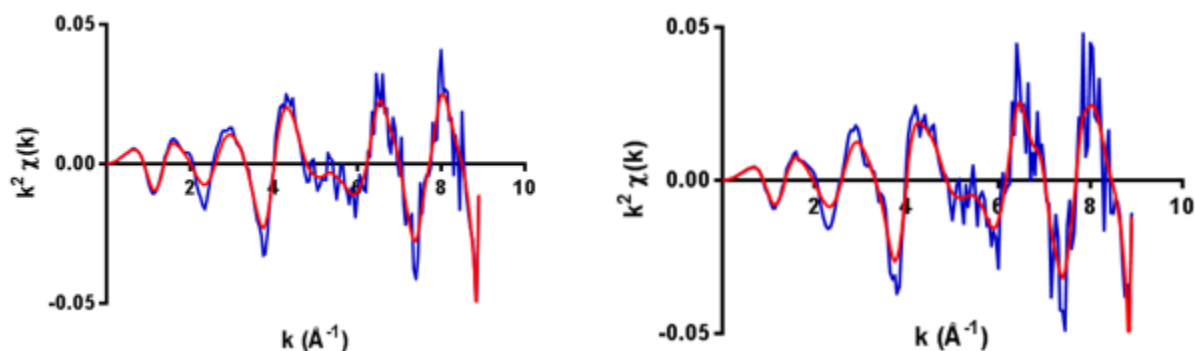


Figure S2 Displaying real and interpolative smoothed data EXAFS data of (Left) $W(CO)_6$ + PFMCH under xenon and (right) $W(CO)_6$ + PFMCH under xenon.

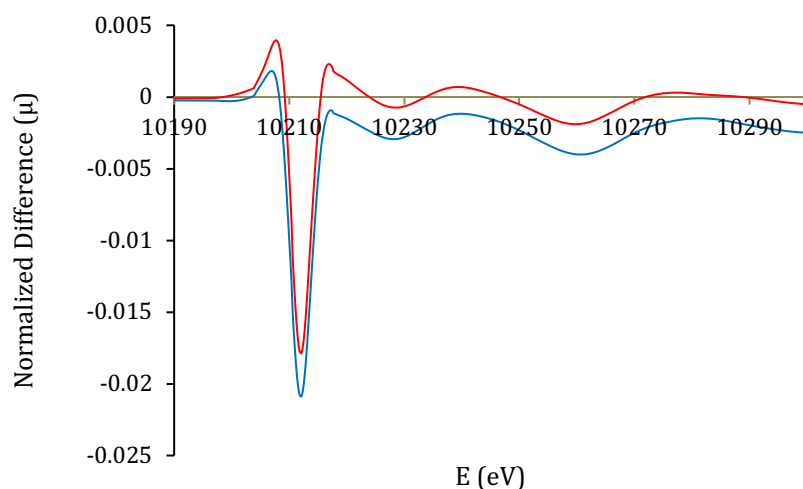


Figure S3 W L_{III} Edge XAS and difference spectra after 30 μs of $W(CO)_6$ + heptane (Blue) and doped $HSiBu_3$ (Red).

Table S1 Distances and fitting parameters of $[W(CO)_5(\text{heptane})]$ from the photolysis of L_{III} edge EXAFS of $W(CO)_6$ in heptane over 30 μs (MS = Multiple scattering).

Paths (ligand)	Variable	Fit determined R (\AA)
1 <i>trans</i> W-C (CO)	$\Delta R = -0.02(1)$	1.94(1) (<i>Trans</i>)
4 <i>cis</i> W-C (CO)	$\sigma^2 = 0.007(1)$	2.03(1) (<i>Cis</i>)
1 W-C (heptane)	$\Delta R = -0.09(6)$ $\sigma^2 = 0.007(12)$	3.07(6)

- Fixed Paths: 6 W-O + W-CO (MS) at 3.13 – 3.21 \AA , $\sigma^2 = 0.002$.
- Laser off $[W(CO)_6]$ – Fixed: $S_0^2 = -0.0190$, $E_0 = 11$ eV, 6 W-C = 2.07 \AA , 6 W-O = 3.22 \AA , 18 W-CO(MS) = 3.22 \AA , $\sigma^2 = 0.001$ for all paths.
- Fit parameters: $S_0^2 = 0.0190(1)$, $E_0 = 9$ eV, R-factor = 0.006, k -range = 2 – 8 \AA^{-1} , k -weighting = 2; R-range = 1.35 – 3.5 \AA . Fitting window = Hanning.

Table S2 Distances and fitting parameters of $[W(CO)_5(HSiBu_3)]$ from the photolysis of L_{III} edge EXAFS of $W(CO)_6$ + $HSiBu_3$ in heptane over 50-75 μs (MS = Multiple scattering).

Paths (ligand)	Variable	Fit determined R (\AA)
1 <i>trans</i> W-C (CO)	$\Delta R = 0.01(1)$	2.01(1) (<i>Trans</i>)
4 <i>cis</i> W-C (CO)	$\sigma^2 = 0.001(2)$	2.06(1) (<i>Cis</i>)
1 W-Si ($HSiBu_3$)	$\Delta R = -0.00(3)$ $\sigma^2 = 0.001(8)$	3.20(3)

- *Fixed Paths:* 6 W-O + X W-CO (MS) at 3.18 – 3.23 Å, $\sigma^2 = 0.002$.
- *Laser off* [$W(CO)_6$] – *Fixed:* $S_0^2 = -0.03$, $E_0 = 11$ eV, 6 W-C = 2.07 Å, 6 W-O = 3.23 Å, 18 W-CO(MS) = 3.23, $\sigma^2 = 0.001$ for all paths.
- *Fit parameters:* $S_0^2 = 0.03(1)$, $E_0 = 9$ eV, R-factor = 0.024, k -range = 3 – 8 Å⁻¹, k -weighting = 2,3; R-range = 1.35 – 3.3 Å. Fitting window = Hanning.

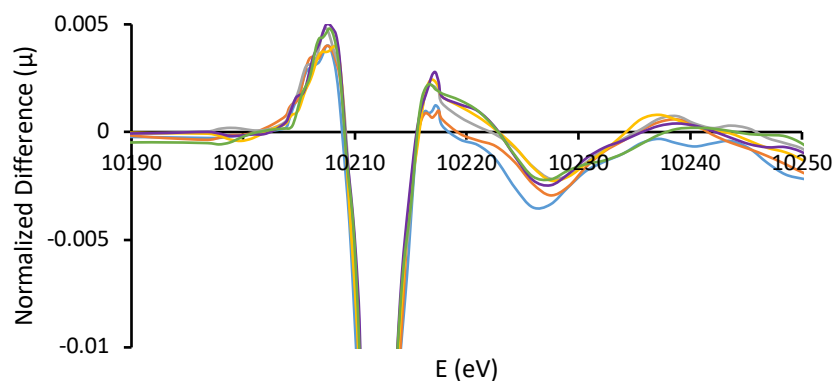


Figure S4 Difference spectra of the photolysis of $W(CO)_6 + HSiBu_3$ at 266 nm in heptane over the first 12 μs showing window of fitting analysis [blue = 0-2 μs ; orange = 2-4 μs ; grey = 4-6 μs ; yellow = 6-8 μs ; purple = 8-10 μs ; green = 10-12 μs].

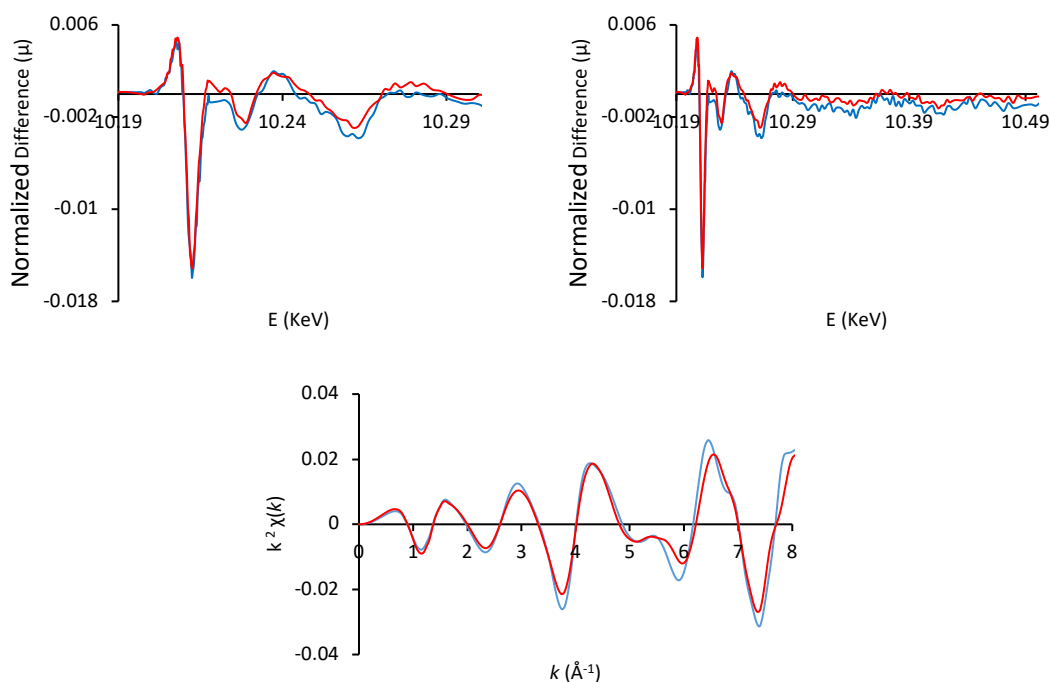


Figure S5 W L_{III} Edge XAS and difference spectra after 4 μs , and extracted EXAFS after 8 μs of $W(CO)_6 + PFMCH$ under helium (blue) and xenon (red).

Table S3 Distances and fitting parameters of [$W(CO)_5(Xe)$] from photolysis of L_{III} edge EXAFS of $W(CO)_6$ in PFMCH under xenon over the first 8 μs after laser flash (MS = Multiple scattering).

Paths (ligand)	Variable	Fit determined R (Å)
1 <i>trans</i> W-C (CO)	$\Delta R = 0.003(6)$	1.96(1) (<i>Trans</i>)
4 <i>cis</i> W-C (CO)	$\sigma^2 = 0.001(1)$	2.06(1) (<i>Cis</i>)
1 W-Xe (xenon)	$\Delta R = 0.026(2)$ $\sigma^2 = 0.002(4)$	3.10(5)
1 <i>trans</i> W-O	$\Delta R = 0.002(4)$	3.11(1)
4 <i>cis</i> W-O	$\sigma^2 = 0.001(1)$	3.20(1)

31 W-CO (MS)	3.11(1) – 3.52(1)
--------------	-------------------

- *Laser off* [$W(CO)_6$] - Fixed: $S_0^2 = -0.065$, $E_0 = 11$ eV, 6 W-C = 2.08 Å, 6 W-O = 3.21 Å, 42 W-CO(MS) = 3.21 – 3.56 Å, $\sigma^2 = 0.001$ for all paths.
- *Fit parameters*: $S_0^2 = 0.065$ (Fix), $E_0 = 7.8$ (Fix) eV, R-factor = 0.003, k -range = 3.5 – 8.2 Å⁻¹, k -weighting = 3; R-range = 1.6 – 3.8 Å. Fitting in R window = Hanning.

Table S4 Distances and fitting parameters of $[W(CO)_5(PFMCH)]$ from L_{III} edge EXAFS of $W(CO)_6$ in PFMCH under helium over the first 8 μ s after laser flash (MS = Multiple scattering).

Paths	Variable	Fit determined R (Å)
1 <i>trans</i> W-C (CO)	$\Delta R = -0.05(1)$	1.97(1) (<i>Trans</i>)
4 <i>cis</i> W-C (CO)	$\sigma^2 = 0.006(2)$	2.05(1) (<i>Cis</i>)
1 W-F	$\Delta R = 0.07(6)$ $\sigma^2 = 0.013(10)$	2.65(6)

- *Fixed Paths*: 5 W-O at 3.12 – 3.19 Å, $\sigma^2 = 0.001$; 34 W-CO(MS) 3.12 – 3.57 Å, $\sigma^2 = 0.001$; 27 W-CO (MS) at 3.98 – 4.77 Å, $\sigma^2 = 0.008$.
- *Laser off* [$W(CO)_6$] - Fixed: $W(CO)_6$: $S_0^2 = -0.03$, $E_0 = 11$ eV, 6 W-C = 2.08 Å, 6 W-O = 3.21 Å, 300 W-CO(MS) = 3.21 – 5.04 Å, $\sigma^2 = 0.001$ for all paths.
- *Fit parameters*: $S_0^2 = 0.03(1)$, $E_0 = 6.6$ eV, R-factor = 0.017, k -range = 3 – 8 Å⁻¹, k -weighting = 1,2,3; R-range = 1.6 – 4.5 Å. Fitting window = Hanning.

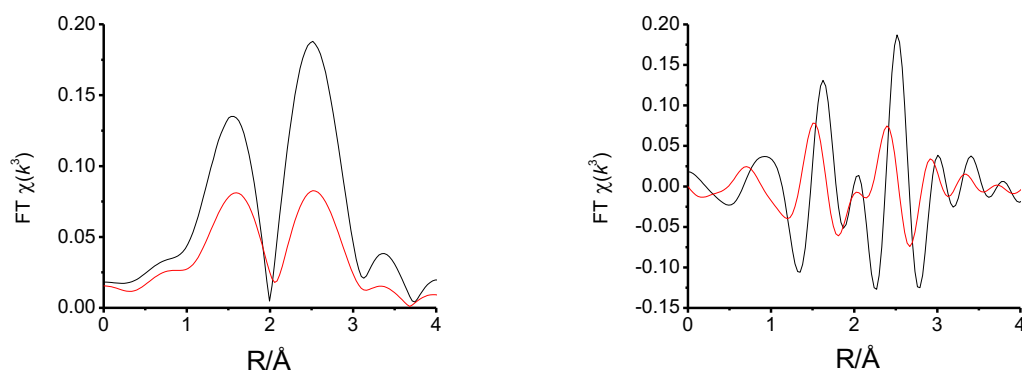


Fig. S6 Comparison of the Fourier transform of the two optimized models of $W(CO)_5Xe$ (Blue) and $W(CO)_5(PFMCH)$ (Red) as defined by the EXAFS fitting analyses (k^3 weighting for k -range 3 – 8 Å⁻¹).

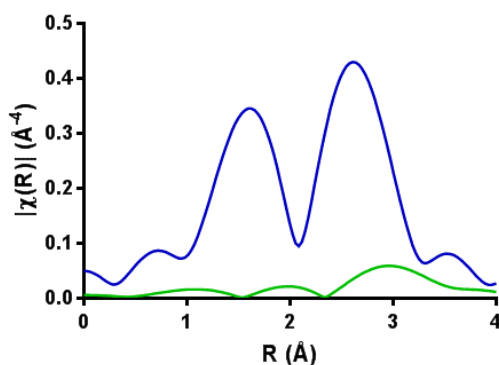


Fig. S7 Displaying the Fourier transform of the derived model from the EXAFS fitting analysis of $W(CO)_5Xe$ (blue) with W-Xe path contribution (green) (k -range 3.5 – 8.2, in k -weighting 3).

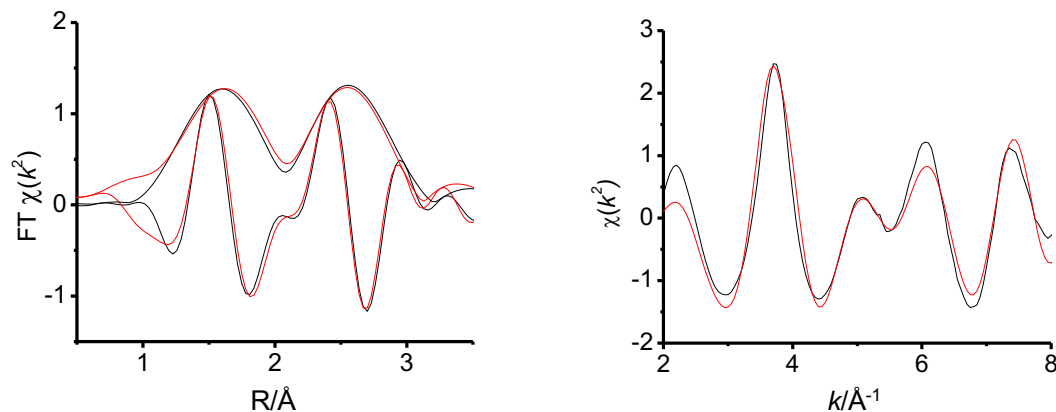


Fig. S8 Displaying the W L_{III} edge EXAFS analysis of before laser/ ground state spectrum of $W(CO)_6$ in heptane, with the EXAFS data (Black) and fit analysis (Red). $W(CO)_6$: $S_0^2 = 0.86$, $E_0 = 11(2)$ eV, 6 W-C = $2.07(2)$ Å; 6 W-O = $3.21(2)$ Å, 300 W-CO(MS) = $3.21 - 5.04$ Å, $\sigma^2 = 0.001$ for all paths.

References

- [S1] Zhao, Y.; Truhlar, D. G. The M06 suite of density functionals for main group thermochemistry, thermochemical kinetics, noncovalent interactions, excited states, and transition elements: two new functionals and systematic testing of four M06-class functionals and 12 other functionals *Theor. Chem. Acc.* **2008**, *120*, 215.
- [S2] Shao, Y. H.; Gan, Z. T.; Epifanovsky, E.; Gilbert, A. T. B.; Wormit, M.; Kussmann, J.; Lange, A. W.; Behn, A.; Deng, J.; Feng, X. T.; Ghosh, D.; Goldey, M.; Horn, P. R.; Jacobson, L. D.; Kaliman, I.; Khaliullin, R. Z.; Kus, T.; Landau, A.; Liu, J.; Proynov, E. I.; Rhee, Y. M.; Richard, R. M.; Rohrdanz, M. A.; Steele, R. P.; Sundstrom, E. J.; Woodcock, H. L.; Zimmerman, P. M.; Zuev, D.; Albrecht, B.; Alguire, E.; Austin, B.; Beran, G. J. O.; Bernard, Y. A.; Berquist, E.; Brandhorst, K.; Bravaya, K. B.; Brown, S. T.; Casanova, D.; Chang, C. M.; Chen, Y. Q.; Chien, S. H.; Closser, K. D.; Crittenden, D. L.; Diedenhofen, M.; DiStasio, R. A.; Do, H.; Dutoi, A. D.; Edgar, R. G.; Fatehi, S.; Fusti-Molnar, L.; Ghysels, A.; Golubeva-Zadorozhnaya, A.; Gomes, J.; Hanson-Heine, M. W. D.; Harbach, P. H. P.; Hauser, A. W.; Hohenstein, E. G.; Holden, Z. C.; Jagau, T. C.; Ji, H. J.; Kaduk, B.; Khistyayev, K.; Kim, J.; Kim, J.; King, R. A.; Klunzinger, P.; Kosenkov, D.; Kowalczyk, T.; Krauter, C. M.; Lao, K. U.; Laurent, A. D.; Lawler, K. V.; Levchenko, S. V.; Lin, C. Y.; Liu, F.; Livshits, E.; Lochan, R. C.; Luenser, A.; Manohar, P.; Manzer, S. F.; Mao, S. P.; Mardirossian, N.; Marenich, A. V.; Maurer, S. A.; Mayhall, N. J.; Neuscammen, E.; Oana, C. M.; Olivares-Amaya, R.; O'Neill, D. P.; Parkhill, J. A.; Perrine, T. M.; Peverati, R.; Prociuk, A.; Rehn, D. R.; Rosta, E.; Russ, N. J.; Sharada, S. M.; Sharma, S.; Small, D. W.; Sodt, A. Advances in molecular quantum chemistry contained in the Q-Chem 4 program package *Mol. Phys.* **2015**, *113*, 184.
- [S3] Roy, L. E.; Hay, P. J.; Martin, R. L. Revised basis sets for the LANL effective core potentials *J. Chem. Theory Comput.* **2008**, *4*, 1029.
- [S4] Chien, S. H.; Gill, P. M. W. SG-0: A small standard grid for DFT quadrature on large systems *J. Comput. Chem.* **2006**, *27*, 730.
- [S5] Gill, P. M. W.; Johnson, B. G.; Pople, J. A. A standard grid for density-functional calculations *Chem. Phys. Lett.* **1993**, *209*, 506.
- [S6] Boese, A. D.; Klopper, W.; Martin, J. M. L. Anharmonic force fields and thermodynamic functions using density functional theory *Mol. Phys.* **2005**, *103*, 863.
- [S7] Merrick, J. P.; Moran, D.; Radom, L. An evaluation of harmonic vibrational frequency scale factors *J. Phys. Chem. A* **2007**, *111*, 11683.
- [S8] König, C. F. J.; van Bokhoven, J. A.; Schildhauer, T. J.; Nachttegaal, M. Quantitative Analysis of Modulated Excitation X-ray Absorption Spectra: Enhanced Precision of EXAFS Fitting *J. Phys. Chem. C*, **2012**, *116*, 19857.
- [S9] Ravel, B. "Quantitative EXAFS analysis," in *X-Ray Absorption and X-Ray Emission Spectroscopy: Theory and Applications*, edited by J. A. van Bokhoven and C. Lamberti (John Wiley & Sons, Ltd., Chichester, UK, 2016), pp. 281–302.